NASA TECHNICAL NOTE

NASA TN D-6803

DETERMINATION OF PILOT AND VEHICLE DESCRIBING FUNCTIONS FROM THE GEMINI-10 MISSION

by Frederick G. Edwards

Ames Research Center
Moffett Field, Calif. 94035

NATIONAL AERONAUTICS AND SPACE ADMINISTRATION • WASHINGTON, D. C. • MAY 1972

1. Report No.	2. Government Accession No.	3. Recipient's Catalog No.
NASA TN D-6803		

4. Title and Subtitle	5. Report Date
DETERMINATION OF PILOT AND VEHICLE DESCRIBING FUNCTIONS FROM THE GEMINI-10 MISSION	May 1972
	6. Performing Organization Code
7. Author(s)	8. Performing Organization Report No.
Frederick G. Edwards	A-3877
	10. Work Unit No.
9. Performing Organization Name and Address	125-17-10-09-00-21
NASA Ames Research Center Moffett Field, California 94035	11. Contract or Grant No.
	13. Type of Report and Period Covered
12. Sponsoring Agency Name and Address	Technical Note
National Aeronautics and Space Administration Washington, D. C. 20546	14. Sponsoring Agency Code

15. Supplementary Notes

16. Abstract

Three types of manual control maneuvers conducted during the Gemini-10 mission have been analyzed in order to measure and document the describing function of the pilot, the vehicle and the pilot-vehicle combination during an actual space mission. Measurements made from the data records of the reentry maneuver (a single axis control task) indicate that the pilot's control behavior changes during critical portions of the reentry. Measurements made of the deorbit maneuver and of a terminal phase initiation maneuver (three axis tasks) show that the pilot assigns priorities to the separate axes and controls them differently. His control technique is also influenced by the magnitude of the thrust disturbance present during the maneuvers. The results for all three types of maneuvers show that the pilot adapts to the nonlinear spacecraft control system in such a way that the combined pilot-vehicle dynamics take the form of the linear "crossover model."

17. Key Words (Suggested by Author(s))	18. Distribution Statement
Identification Pilot dynamics Flight test data Pilot describing function Space vehicles	Unclassified – Unlimited

19. Security Classif. (of this report)	20. Security Classif. (of this page)	21. No. of Pages	22. Price*
Unclassified	Unclassified	42	$3.00

*For sale by the National Technical Information Service, Springfield, Virginia 22151

TABLE OF CONTENTS

NOTATION

$C_x(\tau)$	autocovariance function of the signal x(t)
$C_{xy}(\tau)$	cross covariance function between two signals x(t) and y(t)
c(t)	controller deflection (output of pilot)
dB	$20 \log_{10}$ (amplitude)
e(t)	error signal (input to pilot)
i(t)	external disturbance
K_c	constant gain (controlled element)
K_p	constant gain (pilot)
m(t)	vehicle attitude signal
N	number of data samples in the window, $W/\Delta t$
n(t)	internal noise (pilot remnant)
$R_{ec}(\tau)$	cross-correlation function of e(t) and c(t)
$R_x(\tau)$	autocorrelation function of the signal x(t)
$R_{xy}(\tau)$	cross-correlation function between two signals x(t) and y(t)
r(t)	vehicle rate signal
T_c	lag time constant of controlled element describing function, sec^{-1}
T_p	lead time constant of pilot describing function, sec^{-1}
t	time, sec
t_c	center time of data window (data sample)
W	data sample window width, sec
$Y_c(j\omega)$	vehicle describing function
$\hat{Y}_c(j\omega)$	estimated vehicle describing function
$Y_p(j\omega)$	pilot describing function

$\hat{Y}_p(j\omega)$	estimated pilot describing function
$Y_pY_c(j\omega)$	pilot-vehicle describing function
$\widehat{Y_pY_c}(j\omega)$	estimated pilot-vehicle describing function
$Y_v(j\omega)$	describing function of controlled element
$\hat{Y}_v(j\omega)$	estimated describing function of controlled element
$\gamma(\tau)$	normalized cross covariance function, $\gamma_{ec}(\tau) = \frac{R_{ec}(\tau)}{\sigma_e\sigma_c}$
Δt	data sample interval, sec
$\epsilon(t)$	residual
μ	mean value of signal, $\frac{1}{N}\sum_{n=1}^{N} x_n$
ρ^2	linear coherence function, $1 - \frac{\sigma_\epsilon{}^2}{\sigma_c{}^2}$
σ^2	variance of signal, $\frac{1}{N}\sum_{n=1}^{N}(x_n - \mu_x)^2$
τ	lag time, sec
τ_c	time delay in $Y_c(j\omega)$, sec
τ_e	time delay in $Y_pY_c(j\omega)$, sec
τ_p	time delay in $Y_p(j\omega)$, sec
Ψ^2	mean square value of signal, $\frac{1}{N}\sum_{n=1}^{N}(x_n)^2$
ω	frequency, rad/sec
ω_c	crossover frequency, rad/sec
$\|_{dB}$	magnitude, dB
$\sphericalangle$	angle of
$(\,)'$	output of describing function model

Abbreviations

DF	describing function
FDAI	flight directors attitude indicator
RC	rate command
RHC	rotational hand controller
RRC	reentry rate command
TPI	terminal phase initiation

DETERMINATION OF PILOT AND VEHICLE DESCRIBING FUNCTIONS FROM THE GEMINI–10 MISSION

Frederick G. Edwards

Ames Research Center

SUMMARY

Three types of manual control maneuvers conducted during the Gemini-10 mission have been analyzed in order to measure and document the describing function of the pilot, the vehicle and the pilot-vehicle combination during an actual space mission. Measurements made from the data records of the reentry maneuver (a single axis control task) indicate that the pilot's control behavior changes during critical portions of the reentry. Measurements made of the deorbit maneuver and of a terminal phase initiation maneuver (three axis tasks) show that the pilot assigns priorities to the separate axes and controls them differently. His control technique is also influenced by the magnitude of the thrust disturbance present during the maneuvers. The results for all three types of maneuvers show that the pilot adapts to the nonlinear spacecraft control system in such a way that the combined pilot-vehicle dynamics take the form of the linear "crossover model."

INTRODUCTION

Most investigations of human transfer functions are conducted in a laboratory environment on fixed based simulators. This type of study is well controlled, produces consistent results, and has added greatly to the understanding of the behavior of a pilot in a pilot-vehicle control system. Several studies have measured the human transfer function in a flight environment. All of these studies (refs. 1, 2, 3) have been conducted in aircraft. Little work except the brief accounts in references 4, 5, 6, and 7 has been published from analyses of the pilots control behavior during a spacecraft mission.

This study measures the human describing function from data recorded during some routine maneuvers conducted during the Gemini-10 mission. The maneuvers include the atmospheric reentry, the deorbit (or retro), and a portion of a rendezvous (specifically the terminal phase initiation). These three maneuvers characterize three different types of manual control action which are typical during an orbital space mission. The report first introduces the describing function approach and discusses the identification techniques for measuring the describing function of the pilot and vehicle. The approach to selecting appropriate flight records is outlined next, discussing the types of maneuvers of interest and the associated piloting tasks. The report presents the results of the identification of the pilot, the vehicle and the pilot-vehicle combination for the three spacecraft maneuvers. These results are analyzed to determine the pilot's control behavior and the pilot-vehicle dynamics.

Describing Function Analysis

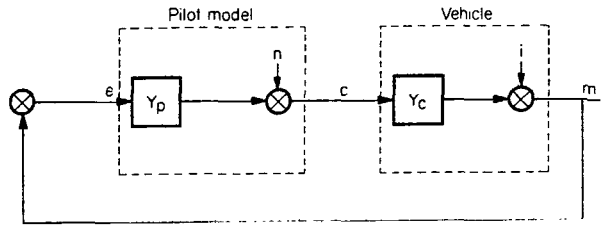

Figure 1.– Pilot-vehicle control system.

Figure 1 is a block diagram of a pilot-vehicle control system. This report considers those types of maneuvers wherein the pilot is in a continuous tracking task trying to control his output c(t) so that the input error e(t) is small. Both the pilot and the vehicle may be nonlinear and time varying.

One way of characterizing the behavior of each element within such closed-loop systems is by quasi-linear models. A quasi-linear model characterizes the system output as the sum of the outputs of a linear term (the describing function)[1] and a remnant term. The remnant term is defined to be linearly uncorrelated with the input signal. In the above figure the pilot is represented by the describing function $Y_p(j\omega)$ and the remnant term n(t). The remnant n(t) represents the difference between the output c(t) of the pilot and the output of the pilot describing function for the specific input e(t). A corresponding representation is made for the vehicle. The vehicle describing function is represented by the linear term $Y_c(j\omega)$ and the remnant term i(t), the difference between the output of the vehicle m(t) and the output of the describing function of the vehicle for the specific input c(t). The function i(t) can account for the nonlinear aspect of the vehicle control system as well as time varying commands and disturbances due to aerodynamics and propulsion. One other describing function that will be of interest in this report is the combination pilot-vehicle system, $Y_pY_c(j\omega)$. The combined system $Y_pY_c(j\omega)$ is not always the same as the product of the two functions $Y_p(j\omega)*Y_c(j\omega)$, because of the nonlinearities of each component.

For this study describing functions will be measured separately for the pilot, $Y_p(j\omega)$, the vehicle, $Y_c(j\omega)$, and the pilot-vehicle combination $Y_pY_c(j\omega)$. The identification of $Y_p(j\omega)$ provides an analytical description of the pilot's control behavior during actual space flight maneuvers. The measurement of $Y_p(j\omega)$ during three different maneuvers permits a quantitative comparison of the pilot's behavior for maneuvers that are typical of orbital space missions. The identification of the open loop $Y_pY_c(j\omega)$ provides understanding of the closed loop piloting task. The nature of $Y_pY_c(j\omega)$ determines the dominant closed loop modes and responses. The pilot-system stability is determined by its gain and phase characteristics.

The describing function modeling technique makes it possible to measure the pilot's behavioral characteristics in control system terms to provide a basis for understanding pilot control actions.

Techniques for Measuring Describing Functions

There have been a variety of techniques developed in recent years for identifying the dynamic character (i.e., describing function) of the human pilot and control system. Among the techniques

[1] The term describing function as used in this report refers to a random input describing function rather than sinusoidal input describing function because random signals are used here (see ref. 8).

are three that were used in this study. These have been referred to in the literature as cross correlation analysis (refs. 9, 10), orthogonal exponential function analysis (refs. 9, 11), and parameter model method (refs. 9, 12). These are time domain measurement methods that evaluate the impulse response function of the system being identified. The dynamic characteristics of a system are described by a frequency response function $Y(j\omega)$, which is defined as the Fourier transform of the impulse response function. In this report the results from the cross correlation and the orthogonal exponential function identification procedures will be presented in the form of frequency response plots (Bode plots) of amplitude ratio and phase angle. The parameter model method evaluates a frequency response function. Thus, the results will appear as analytical expressions.

The three identification methods differ in the constraints placed on the describing function model. The cross correlation method is the least constrained and assumes only that the describing function is physically realizable and has a finite memory length. The orthogonal exponential function method uses a more constrained model and, in addition, assumes that the describing function can be represented by a finite series of orthogonal filters. The most constrained model is used with the parameter model method which assumes that the describing function can be represented by a specific model (either first or second order).

All of the methods were used in this report with a unique feature known as "time shifting." This process (refs. 5, 6, 7, 13) represents only a slight modification to the normal use of the identification methods. In effect, the system input is shifted with respect to the output during the computer processing by an amount equal to the time delay of the pilot (or system). This technique of time shifting was originally presented in reference 5 where the process was shown to reduce the measurement error for systems where the primary disturbance is internal to the control loop. For space flight maneuvers such as those analyzed in this study, the major disturbance to the control loop is due to the pilot remnant (pilot's output noise) and the control system propulsive disturbances. The use of time shifting allows a more accurate identification of the describing function for either the pilot or the control system.

The procedure for using the identification schemes will be discussed briefly for the three system elements: the pilot, the vehicle, and the pilot-vehicle combination. Figure 2 shows diagrammatically the manner in which the pilot identification was performed. The identification process determines the estimate $\hat{Y}_p(j\omega)$ which minimizes the difference between the model output C′ and the actual output C. In general, the model will not account for all of the output of the pilot. The part not accounted for, which is called the residual $\epsilon(t)$, is the difference between the actual output c(t) and the model output c′(t).

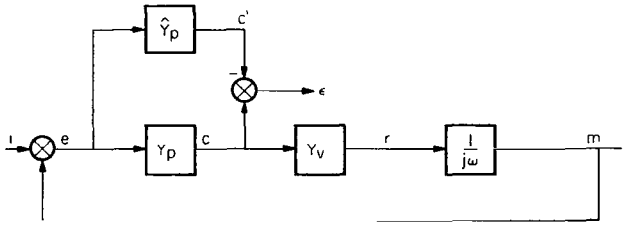

Figure 2.– Scheme for pilot identification.

A particularly valuable piece of information provided by the identification scheme is the linear coherence function, ρ^2. The linear coherence defined as

$$\rho^2 = \frac{\sigma_c^2 - \sigma_\epsilon^2}{\sigma_c^2} \quad \text{or} \quad 1 - \frac{\sigma_\epsilon^2}{\sigma_c^2} \tag{1}$$

is a measure of the ratio of the linearly correlated output of the model to the total output of the pilot. The values of ρ^2 can range from nearly zero to nearly one.

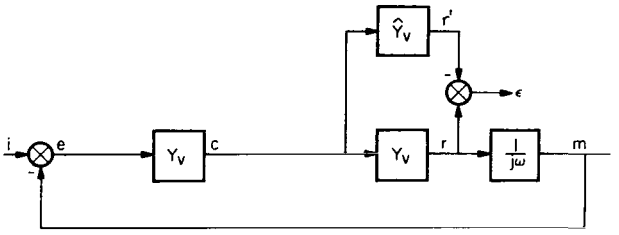

Figure 3.– Scheme for vehicle identification.

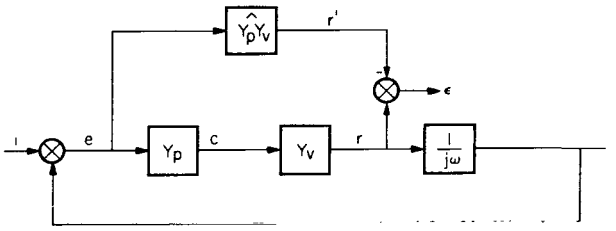

Figure 4.– Scheme for pilot-vehicle identification.

The identification of the vehicle is carried out in much the same manner as described above for the pilot identification. The process is shown diagrammatically in figure 3.

The identification was made between the input signal to the vehicle (pilots output signal c(t)) and the attitude rate signal r(t) from the vehicle.[2] Using these two signals requires that the complete vehicle describing function be defined as:

$$\hat{Y}_C(j\omega) = \hat{Y}_V(j\omega) \cdot \frac{1}{j\omega}$$

The identification of the pilot-vehicle combination was measured between the attitude error signal e(t) and the attitude rate signal r(t), as shown in figure 4. The pilot-vehicle describing function is defined as:

$$\hat{Y}_p\hat{Y}_C(j\omega) = \hat{Y}_p\hat{Y}_V(j\omega) \frac{1}{j\omega}$$

Choosing Records for Analysis

The decision to analyze the flight records from the Gemini missions was made after all of the missions had been flown. The data used for this report were recorded as a normal part of the missions and the astronaut was unaware at the time that his control behavior would be analyzed. In order to limit the number of maneuvers to a reasonable number and to avoid the additional complexity of different pilots, only the data from one mission, Gemini 10 will be analyzed in this report.

The large number of different types of manned maneuvers conducted during the Gemini–10 mission and the consequent lengthy data records made it mandatory to establish a procedure to eliminate at the outset of the study those periods not amenable to the describing function analysis techniques. A study of the mission flight plan and a superficial look at the data eliminated many

[2] The identification between the input and the rate signals, rather than the input and the attitude signals, was used because the methods required that the impulse response of the system being identified return to zero in some finite length of time. A system with a pure integration ($1/j\omega$) does not meet this requirement.

portions from consideration due to incomplete data records or no control activity on the part of the pilot. A more detailed examination of the remaining records was required and was carried out in two phases. The two phases are designated "subjective evaluation" and "quantitative evaluation." The subjective evaluation selects the type of maneuver to analyze, while the quantitative evaluation selects the time span within the maneuver to be analyzed. These two phases are outlined below.

Subjective evaluation of data records– Of most interest to the investigator are those maneuvers that are critical to the success of the mission (i.e., retro, reentry, rendezvous, etc.). These maneuvers are assumed to represent periods where the pilot is conscientiously applying himself to the control task, with few distracting subtasks to be accomplished. If this assumption is correct, the resulting data records for these periods will show a high level of tracking activity (rotational hand controller (RHC) output) and good correlation between the pilots input and output channels. This correlation can be subjectively evaluated by comparing the time histories of the input-output records, and observing corresponding responses in each channel. This process made it possible to reduce the number of maneuvers to be considered to a selective few which appeared to be well correlated tracking examples. The results of the subjective evaluation of the data records was that three maneuvers were chosen to be analyzed: The reentry maneuver, the retro maneuver, and the terminal phase initiation (TPI) maneuver.

Quantitative evaluation of data records– After the initial assessment process established the three maneuvers to be analyzed, the evaluation process was then carried a step farther to select the "best" time period during the maneuver to measure the describing functions. Although the describing functions could have been measured for the total time period of the maneuver, giving the average for that period, it was found that the pilot's control behavior varied considerably during each maneuver. Thus, it was decided that a more representative describing function could be measured if a shorter time period was chosen where the correlation between input-output record was high.

A normalized cross covariance function (ref. 14) was used to evaluate the linear correlation between the input-output record. The normalized cross covariance function is defined as:

$$\gamma_{xy}(\tau) = \frac{R_{xy}(\tau)}{\sigma_x \sigma_y} \tag{2}$$

where $\gamma_{xy}(\tau)$ is between the limits $-1.0 \leqslant \gamma_{xy}(\tau) \leqslant +1.0$. The function $\gamma(\tau)$ measures the degree of linear dependence or linear correlation between x(t) and y(t) for a displacement of τ seconds in y(t) relative to x(t). A high value of $\gamma_{xy}(\tau)$ would indicate a segment of the data record that would be amenable to further analysis. A low value of $\gamma_{xy}(\tau)$ would indicate a record segment that would yield poor results were an attempt made to identify the system relating the two signals. The normalized cross covariance function is discussed in more detail in appendix A where it is shown that the choice of an appropriate τ does not appear to be critical as long as the choice is in the correct range. In the case of an input-output record for a pilot tracking run, $\tau = \tau_p$ and represents the effective time delay of the pilot.[3] For the cases examined in this report, τ_p in the range from 0.3 to 0.8 sec was found to be appropriate. The value $\tau_p = 0.5$ sec was used in the examples presented later. For the vehicle control system, $\tau = \tau_c = 0.2$ sec was used. For records representing

[3]The effective time delay is a low-frequency approximation to all the higher frequency lags in the system. For a control system, this would include response of sensors in the feedback loop or apparent delays due to a nonlinear element (i.e., dead zone). In the case of a pilot the delay is due to neuromuscular lags and transport lags including alternate scanning of display quantities and sequential processing.

the input-output of the pilot-vehicle combination, additive values ($\tau = \tau_p + \tau_c = \tau_e$) would be an effective choice (i.e., $\tau_e = 0.7$ sec). Example of the use of the normalized cross covariance function for evaluating tracking records are given in subsequent sections.

CONTROL SYSTEM DESCRIPTION

General Remarks

Figure 5 is a simplified block diagram of the Gemini vehicle attitude control system. The diagram represents a single axis of the noncoupled three axis system. The forward signal path consists of two nonlinear components and the vehicle dynamics. The threshold network passes signals proportional to the control system input (pilot's output) which are in excess of the dead zone and less than the limiting value. The jet controller is an on-off-on network which activates the vehicle attitude thrusters for signals greater than the dead zone. The vehicle rate is fed back and compared with the input, and the difference is used to control the jet firing. This type of control system is described as a nonlinear rate command system, since the vehicle rate will tend to track the commanded input rate for signals larger than the dead bands. In the absence of a command input, closed loop stabilization of the spacecraft rates is accomplished. Basically the system is highly damped and easily controlled.

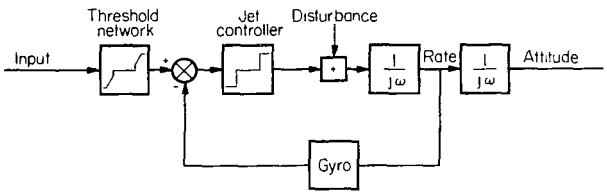

Figure 5.– Gemini vehicle attitude control system.

This control system has several modes of operation that are applicable to the various phases of the Gemini missions. Two of the system modes of interest here are the reentry rate command mode and the rate command mode. These two modes differ in several respects.

Reentry Rate Command Mode

In the reentry rate command (RRC) mode, only a single axis task, the vehicle roll axis, is under manual control. The pitch and the yaw axes are automatically rate damped and do not require inputs from the pilot. The RRC mode is used during the atmospheric reentry of the spacecraft. Figure 6 shows the roll attitude control loop for the RRC mode of operation.

A varying roll angle command signal is generated in the spacecraft digital computer from an estimate of the crossrange and downrange position. The signal commands the direction of the spacecraft's lift vector necessary to steer to a stored reference trajectory which terminates at the target (landing point). The difference between this roll command and the vehicle roll attitude is displayed to the pilot on the flight directors attitude indicator (FDAI) as a roll error signal. The pilot's task is to keep this roll error near zero by inputting signals from the rotational hand controller to the roll control loop of the vehicle. The control technique simultaneously nulls the downrange and crossrange trajectory errors. The pilot flies this lifting trajectory until the spacecraft trajectory coincides with the reference trajectory. At this point, a constant roll rate is commanded

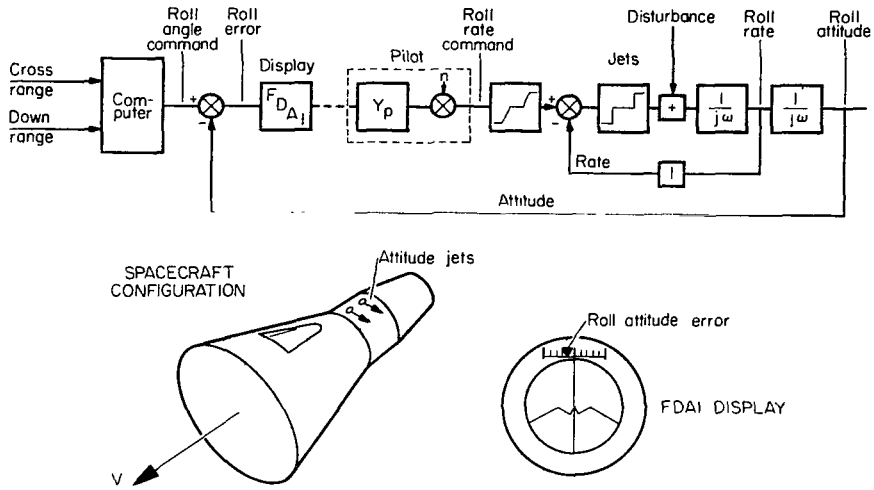

Figure 6.– Roll attitude control for the RRC mode.

to neutralize the effect of the inherent lifting capability of the spacecraft. The rolling portion of the trajectory is interrupted occasionally in order to command any additional lift necessary to steer back to the reference trajectory.

With the system in the RRC mode the effective dead band of the attitude control jets is ±2°/sec. This fairly wide dead band causes the pilot to adopt a somewhat different control behavior than would be expected for control of a rate command system. This fact will be discussed further in a later section.

Rate Command Mode

In the rate command (RC) mode, the attitudes of all three of the spacecraft axes are manually controlled. Two types of spacecraft maneuvers will be analyzed using this control configuration. They are the retro and the terminal phase initiation (TPI) maneuvers. Both are orbital velocity change maneuvers.

A block diagram of the attitude control system for the rate command mode of operation is presented in figure 7. The control loop for each of the three axes is identical and uncoupled. Only

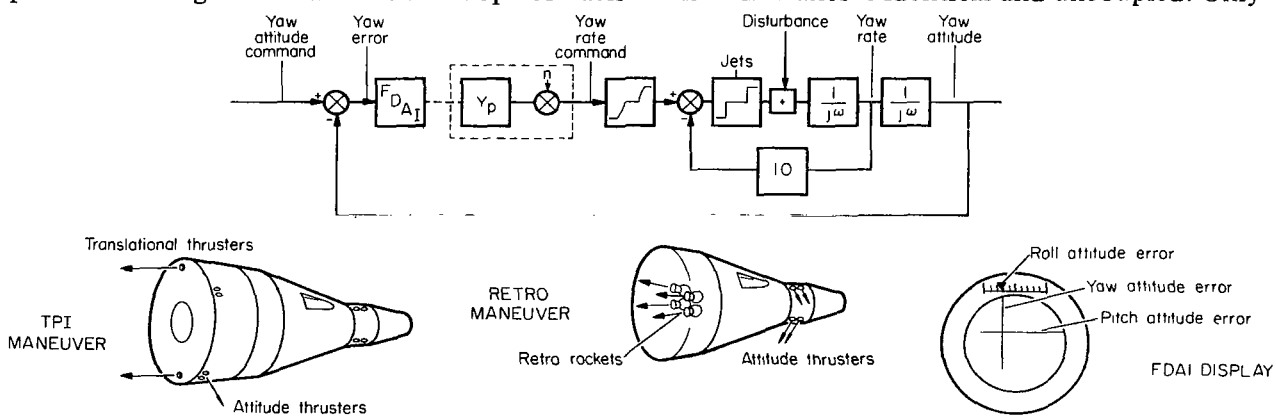

Figure 7.– Attitude control system for the rate command mode.

one axis is shown in the figure. The control loop for the RC mode differs in several ways from the control loop for the RRC mode discussed earlier in the previous section. A principal difference is that the command input signals are invariant. The vehicle is to be controlled to a constant attitude during these orbital velocity change maneuvers. A second difference is that the jet controller effective dead band is reduced to ±0.2°/sec by increasing the rate feedback gain by a factor of 10. The smaller dead band allows more precise control than attainable with the RRC mode where the dead band is ±2°/sec. A third difference is that all three spacecraft axes are under manual control rather than just the roll axis as was the case for the RRC mode.

The pilot's task for the retro and the TPI maneuvers is to control the vehicle about three axes to a constant inertial attitude while an external thrust disturbance is introduced by the rocket engines. Excursions about the constant attitude position are fed to the FDAI and displayed to the pilot as error signals about the pitch, roll, and yaw axes. The pilot inputs signals through his rotational hand controller to reduce these errors. During the retrofire maneuver the external disturbance is caused by the unsymmetrical ripple firing of the four retrorockets. During the TPI maneuver, the disturbance is due to the translational thrusters firing. This type of pilot control problem is a three-axis compensatory tracking task. The pilot's control behavior can be expected to be different for the two velocity change maneuvers since the size of the thrust disturbance is an order of magnitude larger for the retrofire case than during the TPI maneuver.

FLIGHT TEST RESULTS FROM GEMINI 10

As a result of the subjective analysis, three space flight maneuvers were chosen for further analysis: the manually controlled reentry maneuver, the retro maneuver, and the TPI maneuver. During the reentry maneuver, the pilot, using RRC, is controlling only the roll axis of the vehicle while being subjected to the acceleration stresses and atmospheric disturbances of entry. The retro and TPI maneuvers are three-axis pilot control tasks that require similar control.

Reentry Maneuver

A time history of the recorded roll axis data is shown in figure 8. This plot shows four individual segments in which the pilot is in closed loop control of the spacecraft. These are separated by segments in which the vehicle is being rolled at a constant rate to neutralize the effects of the inherent lift of the vehicle. The initial segment of about 100 seconds and the second, much shorter segment, occur prior to peak g. The third segment occurs about peak g. The fourth segment occurs after peak g. A quantitative evaluation of these flight data records was carried out. This computation assisted in the selection of segments of the data records for which the describing function will be identified. A quantitative measure of the linear correlation between the input and output signals of the pilot, the vehicle, and the pilot-vehicle combination was computed in the form of a normalized cross-covariance function. The normalized cross-covariance (γ_{xy}) function was computed by a "sliding window" technique which gives a continuous time history of the function during the reentry maneuver. The sliding window technique is explained in detail in appendix V. It is simply a process for selecting short segments of a long data record for analysis. The time histories of the resulting computations for the input-output records of the pilot (error to control), the

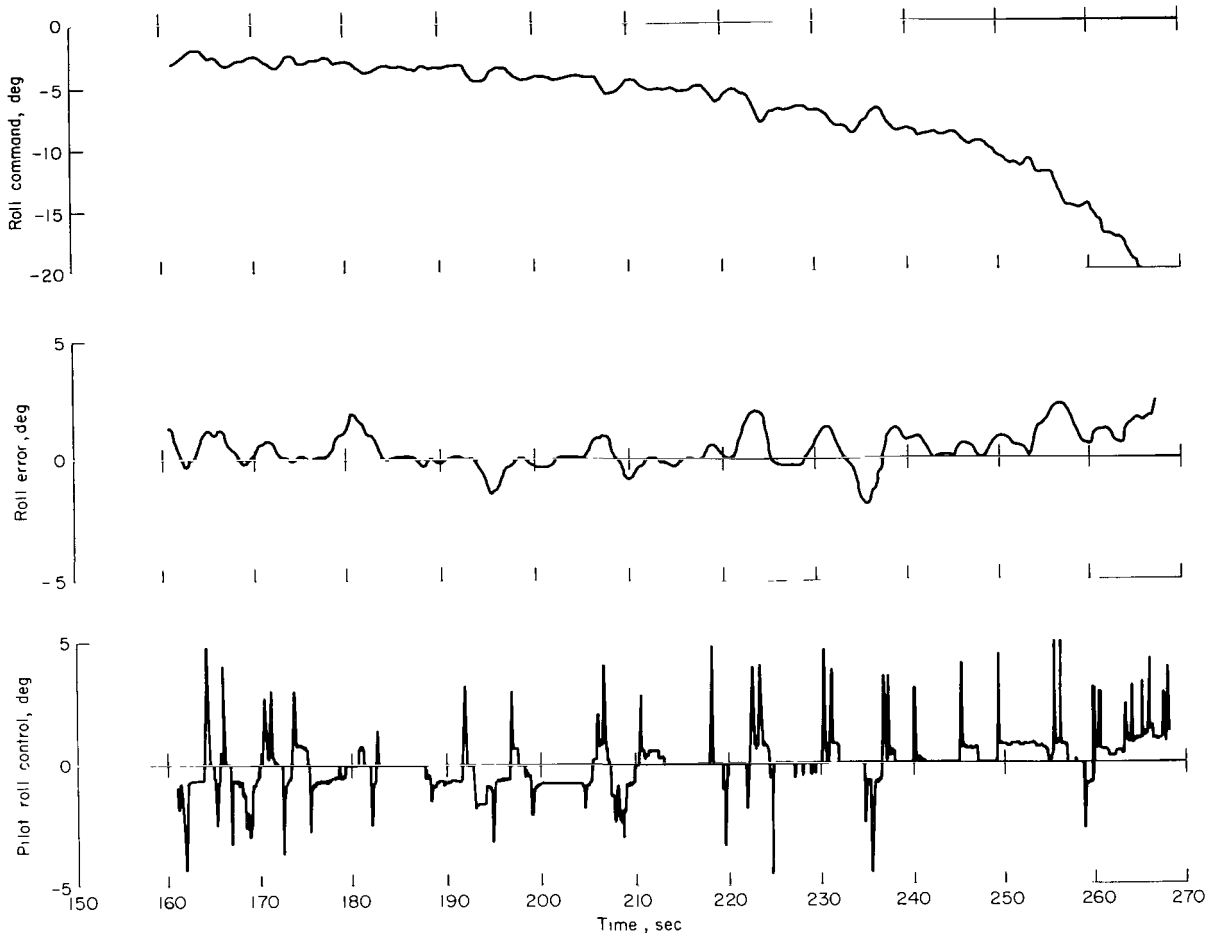

(a) Initial segment.

Figure 8.– Time history of reentry maneuver.

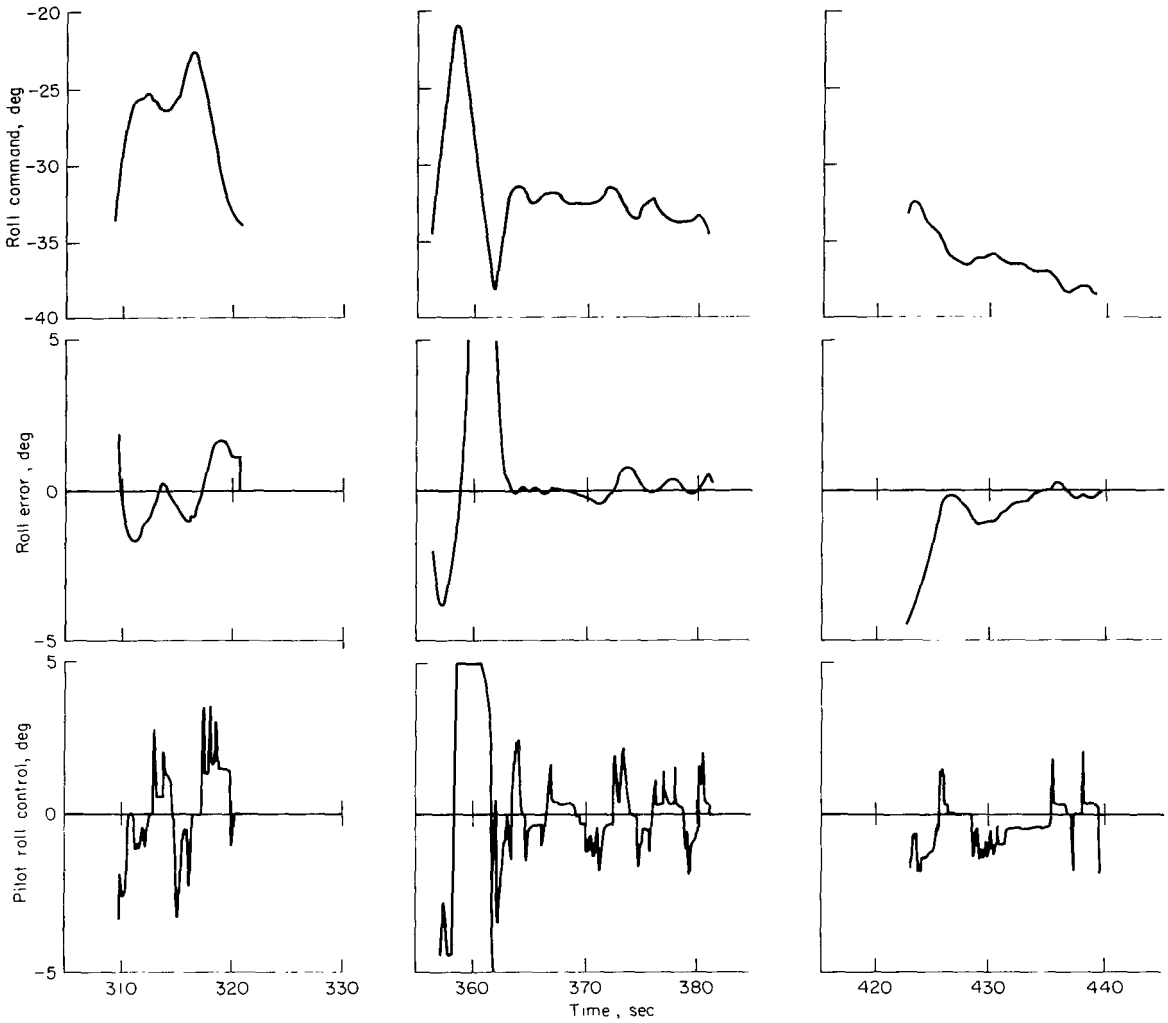

(b) Three later segments of reentry maneuver.

Figure 8.– Concluded.

vehicle (control to rate) and the pilot-vehicle combination (error to rate) are shown in figure 9 for the reentry maneuver. It should be recalled that high values of γ_{xy} indicate which segments of the data records would be amenable to further analysis, while low values of γ_{xy} indicate which record segments would yield poor results were further analysis attempted. It is apparent from the plot that the linear correlations of the input-output records of each of the loop components varies considerably during the maneuver. At times the correlation of the input-output records of the pilot is quite low ($\gamma_{ec} \approx 0.2$) while at other times it is as high as $\gamma_{ec} \approx 0.5$. This time variation can be attributed to the pilot's alternating emphasis on the attitude control task and on other systems management tasks. These variations will be shown to be typical of the pilot's behavior during each of the flight maneuvers to be discussed.

A comparison of the covariance function with the mean squared value of the error signal (Ψ_e^2) during the entry gives further insight into the pilot's control behavior. The mean squared values of the error signal (Ψ_e^2) and the pilot control signal (Ψ_c^2) are presented in the lower part of figure 10. The covariance function for the error to control relationship is reproduced from figure 9 and presented at the top of figure 10.

The magnitude of the Ψ_e^2 and Ψ_c^2 signals vary in cyclic manners similar to the variation of γ_{ec}. But what is interesting is that during segments where the magnitude of the error signal is small (i.e., t_c = 193 sec, diamond symbol ◇). The correlation between the input and output signals is low, indicating that the pilot control activity is either low or his control is incorrectly input. The plot of Ψ_c^2 at this point indicates that the control activity (actually the magnitude of the mean squares value of the pilots inputs) is low. This implies that the pilot is tolerating small attitude dispersions and does not act until the errors exceed some assigned threshold.

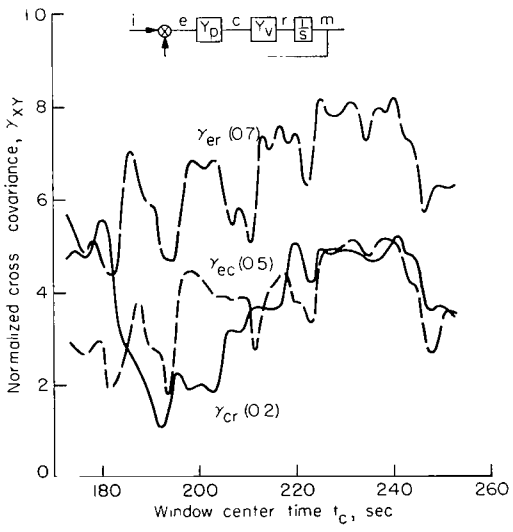

Figure 9.– Linear dependence between output and input signals during reentry maneuver.

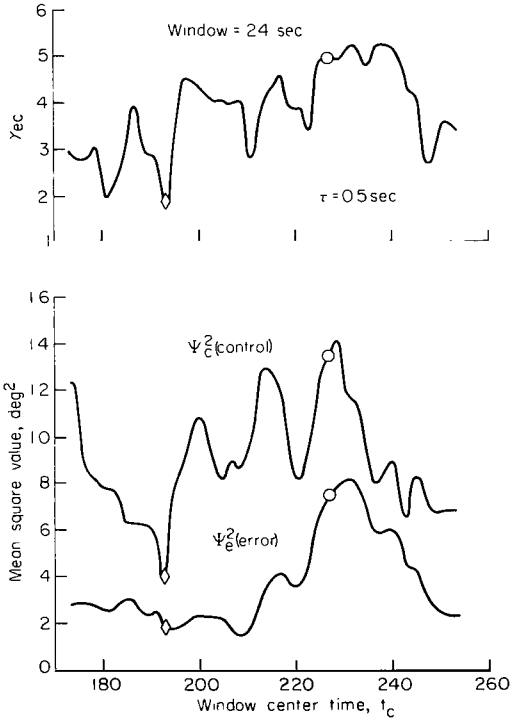

Figure 10.– Comparison of variation of γ_{ec} with mean squared values of signals.

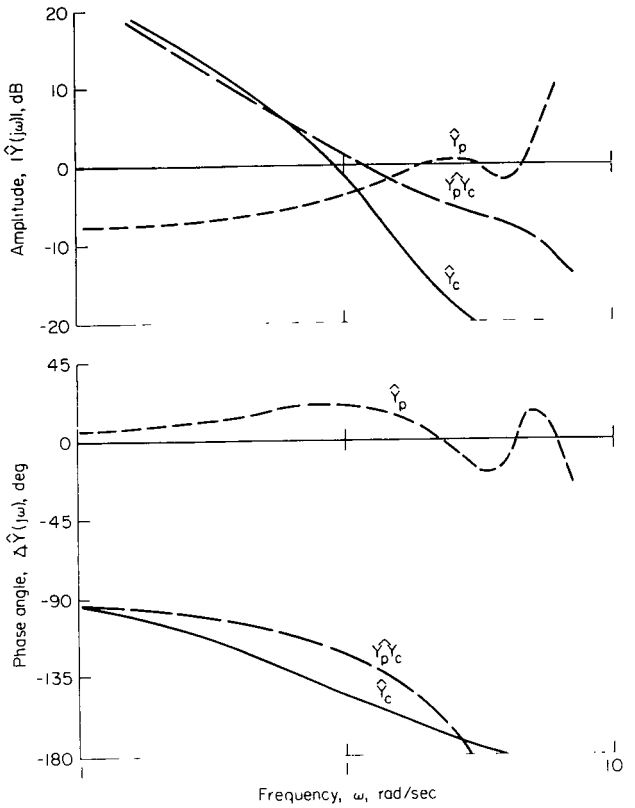

Figure 11.– Identification of describing function during a segment of the reentry maneuver (t_c = 227 sec).

When γ_{ec} for the error signal is large (i.e., t_c = 227 sec, circle symbol ⊙),the control inputs are also large and the correlation between the input and output signal is high.

The periods of high correlation should provide regions where the computation of the pilot, the vehicle, and the combination pilot-vehicle describing function would be meaningful. Measurements of $\hat{Y}_p$, $\hat{Y}_c$, and $\widehat{Y_pY_c}$ were made for the 24-sec region centered at t_c = 227 sec (indicated by the circle in fig. 10). These describing functions are shown in figure 11 and summarized in table 1. In figure 11, curves of magnitude $|\hat{Y}(j\omega)|_{dB}$ and phase angle $\sphericalangle Y(j\omega)$ are presented as a function of frequency. These results were obtained by the orthogonal exponential function identification scheme (refs. 9 and 11). It can be seen from the curve that the estimated describing function for the combination pilot-vehicle can be approximated by the transfer function

$$\widehat{Y_pY_c} = \frac{\omega_c e^{-\tau_e j\omega}}{j\omega} \qquad (3)$$

This form of $\widehat{Y_pY_c}$ is the well known "crossover model" (refs. 5, 6, and 15). It was pointed out in reference 15 that consideration of the requirement of "good" feedback system performance leads directly to the conclusion that the pilot adjusts his describing function so that the open loop function $\widehat{Y_pY_c}$ in the vicinity of the gain crossover region (where $|\widehat{Y_pY_c}|_{dB} = 0.0$), is closely approximated by the crossover model. This model appears to be a good fit to the data presented in figure 11. The frequency at crossover, ω_c, can be seen to be about 1.1 rad/sec. The time delay τ_e is about 0.6 sec. This model implies that the pilot adopts a sufficient lead or lag equilization such that the slope of $|Y_pY_c|_{dB}$ (open loop) is close to -20 dB/decade in the region of the crossover frequency. This same 24-second segment of data was analyzed by the parameter model method (refs. 9-12). The values resulting from the parameter model method in the form of equation (3) were ω_c = 0.78 and τ_e = 0.82. These values of ω_c and τ_c are in fair agreement with the estimates given above for the orthogonal exponential function method.

The describing function for the pilot $\hat{Y}_p$ and the vehicle $\hat{Y}_c$ are also presented in figure 11. The estimated describing function for the pilot can be approximated by a constant gain, a lead term and a time delay:

$$\hat{Y}_p = K_p(T_p j\omega + 1)e^{-\tau_p j\omega} \qquad (4)$$

The parameter model method gives these values at K_p = 0.35, T_p = 1.8, and τ_p = 0.49. The lead term was not anticipated for a pilot controlling this rate command system. Reference 15 indicates

TABLE 1.– SUMMARY OF MEASURED DESCRIBING FUNCTIONS

Axis	$\hat{Y}_p$ General method*	ρ^2	$\hat{Y}_p$ Parameter model	ρ^2	$\hat{Y}_c$ General method*	ρ^2	$\hat{Y}_c$ Parameter model	ρ^2	$\hat{Y_p Y_c}$ General method*	ρ^2	$\hat{Y_p Y_c}$ Parameter model	ρ^2
Reentry maneuver (t_c = 227 sec)												
Roll	Figure 11	0.24	$0.35(1.8j\omega + 1)e^{-0.49j\omega}$	0.18	Figure 11	0.73	$\frac{1.4e^{-0.11j\omega}}{j\omega(1.3j\omega + 1)}$	0.76	Figure 11	0.82	$\frac{0.78e^{-0.82j\omega}}{j\omega}$	0.63
Retromaneuver (t_c = 630 sec)												
Yaw	Figure 15(a)	.67	$1.2e^{-0.59j\omega}$	.66	Figure 15(a)	.72	$\frac{0.51e^{-0.08j\omega}}{j\omega(0.08j\omega + 1)}$	.66	Figure 15(a)	.66	$\frac{1.2e^{-0.72j\omega}}{j\omega}$	.58
Pitch	Figure 15(b)	.73	$4.3(0.7j\omega + 1)e^{-0.67j\omega}$	.70	Figure 15(b)	.41	$\frac{0.22e^{-0.07j\omega}}{j\omega(0.8j\omega + 1)}$	.50	Figure 15(b)	.42	$\frac{0.89e^{-0.77j\omega}}{j\omega}$	.38
Roll	Figure 15(c)	.62	$1.9e^{-1.78j\omega}$	.59	Figure 15(c)	.67	$\frac{0.25e^{-0.18j\omega}}{j\omega(0.09j\omega + 1)}$	.62	Figure 15(c)	.54	$\frac{0.38e^{-2.2j\omega}}{j\omega}$	.47
Terminal phase initiation maneuver (t_c = 797 sec)												
Yaw	Figure 19(a)	.60	$5.2e^{-1.1j\omega}$	.53	Figure 19(a)	.43	$\frac{0.11e^{-0.14j\omega}}{j\omega(0.06j\omega + 1)}$	.46	Figure 19(a)	.22	$\frac{0.43e^{-1.3j\omega}}{j\omega}$	.17
Pitch	Figure 19(b)	.26	$2.3(0.7j\omega + 1)e^{-1.3j\omega}$	.23	Figure 19(b)	.55	$\frac{0.14e^{-0.16j\omega}}{j\omega(0.09j\omega + 1)}$	.52	Figure 19(b)	.17	$\frac{0.47e^{-1.5j\omega}}{j\omega}$	.16
Roll	Figure 19(c)	.33	$0.53e^{-1.7j\omega}$	.33	Figure 19(c)	.55	$\frac{0.41e^{-0.08j\omega}}{j\omega(0.11j\omega + 1)}$	.55	Figure 19(c)	.68	$\frac{0.41e^{-1.8j\omega}}{j\omega}$	.68

*General method means either the orthogonal exponential function or the cross-correlation identification techniques.

that the form of the pilot for controlling a pure rate command system should be $\hat{Y}_p = K_p e^{-\tau_p j\omega}$ However, the difference in the example presented here is that the vehicle control system incorporates a wide dead-band nonlinear element which effectively reduces the gain in the rate feedback loop.[4] Consequently, the response of the vehicle is reduced over a portion of the frequency spectrum. Reference to figure 11, which shows the measured describing function of the vehicle, will help clarify this point. The describing function of the vehicle may be approximated by the transfer function

$$\hat{Y}_c = \frac{K_c e^{-\tau_c j\omega}}{j\omega(T_c j\omega + 1)} \tag{5}$$

When the parameter model method is used to evaluate the parameters of equation (5), the results show that the first order lag term has a break frequency in the crossover region ($1/T_c = 0.8$). As a result, the pilot is required to adopt sufficient lead to compensate for this lag term in order to achieve good close loop system response. The time delay term (τ_c) in equation (5) is associated with the actuation, build-up, and decay of the jet thruster. Its average measurement was about 1/10 sec during this maneuver. The gain value K_c was estimated to be about 1.4.

It is noted that fluctuations appear in the describing functions in the frequency range above 4 rad/sec. This is attributed to the very low power existing in the input error signal at these higher frequencies. The identification schemes cannot make a proper identification over the range of frequencies where the very low power exists. The describing functions presented in figure 11 are actually valid over a limited range of frequencies from the low end at about 0.3 rad/sec to the upper end of about 4 rad/sec. The lower limit of the frequency range results from the choice of the data sample length (W = 24 sec for these examples) while the upper limit is due to the very low power existing in the signals above 4 rad/sec. The results from the analysis of the reentry maneuver are summarized in table 1. The results from the parameter model method are given as analytical expressions. The result from the general methods (cross correlation and orthogonal exponential functions) are referred to by the figure numbers in the table. A measure of the linear coherence (ρ^2) is given in table 1 for each computation. These values were computed by means of equation (1). Generally, the coherence is less for the parameter model than for the general model methods since the form of the parameter models is more restrictive. When ρ^2 for a general method and the parameter model method are approximately equal (even though low valued), it indicates that the simpler parameter model is as good a linear representation of the input-output relationship as is possible. When the values of linear coherence are widely different for the two methods the indication is that a more complex parameter model than is used in this report is required to describe the input-output relationship. In table 1 for the reentry maneuver ρ^2 for the parameter and general methods agree closely (within 0.2) indicating that the chosen form of the parameter models is a reasonable linear representation of the actual processes that have taken place.

To obtain a picture of the pilot changing control behavior during the reentry and its effect on the pilot-vehicle response, the pilot-vehicle crossover frequency and effective time delay were computed as a function of time, from the time of guidance initiation until termination. The parameter model identification scheme was used for this computation. The model was in the form of equation (3), "the crossover model." The parameters (ω_c, τ_e) of the $\hat{Y}_p\hat{Y}_c$ model were computed for each position of the window using the sliding window technique. The results, presented in figure 12, are plotted versus the center time of the window.

[4] Actually, the wide dead band is a result of the low gain in the rate loop (see fig. 6).

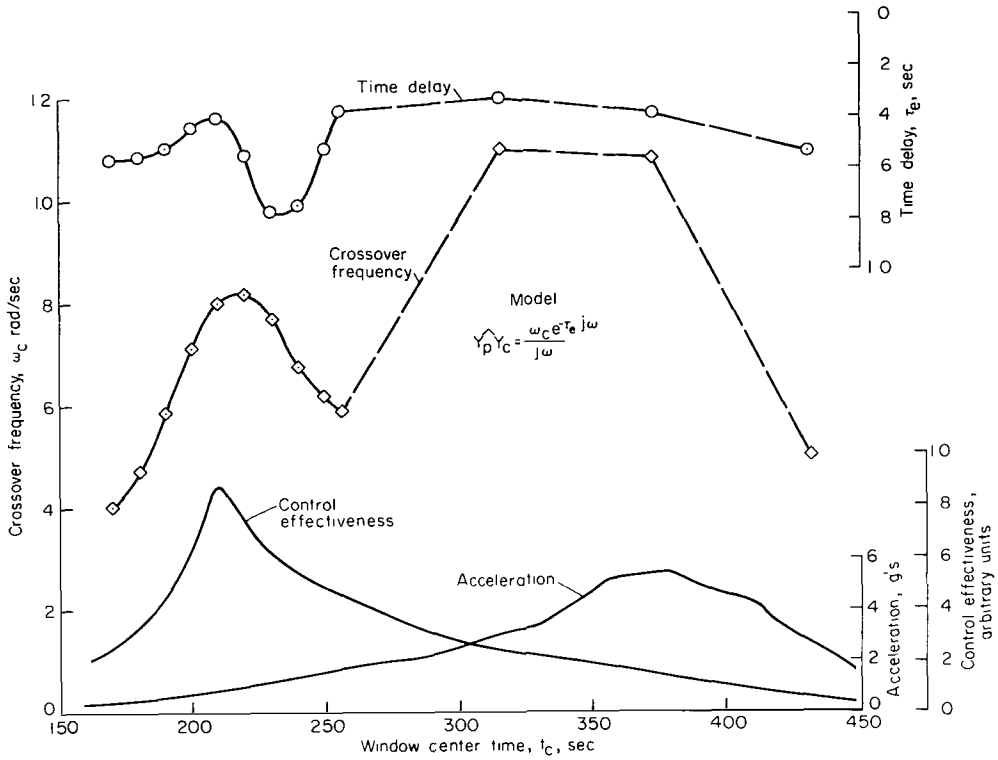

Figure 12.– Comparison of model parameters with flight parameters during reentry.

The parameters ω_c and τ_e reflect, to some degree, the effort that the pilot is expending during the control task. In general, shorter time delays and higher crossover frequency infer more active tracking and better performance (ref. 8). Thus, it would be reasonable to expect that a trend would appear in the time histories of these parameters which would be related to either the environmental acceleration or the control effectiveness of the spacecraft. Whereas the acceleration is actually sensed by the pilot, he is only indirectly aware of the spacecraft control effectiveness. Preflight training has made him aware that during the early portion of the entry, the vehicle control effectiveness is higher; thus, the attitude control problem is more critical to mission success (landing point dispersion) than during the later portion. Approximately 80 percent of the vehicle maneuvering capability is expended during the first 50 percent of the reentry (between 250,000 and 170,000 ft altitude). Thus, his performance may reflect his awareness of this difference. To facilitate a comparison, the time histories of reentry acceleration and vehicle control effectiveness are also presented in figure 12.

No apparent correlation is evident between either ω_c or τ_e and the entry acceleration. Actually this result is consistent with the results of reference 16 which show that for an "easy task" (well damped vehicle) performance is unaffected for sustained acceleration levels less than about 6 g. Thus it is not surprising that no effects are evident for this reentry acceleration profile which is not sustained but gradually built up and peaks at less than 6 g.

What is more apparent from figure 12 is the gradual buildup and decay in the crossover frequency during the early phase of the entry ($t_c < 260$ sec). The curve of ω_c parallels the curve of vehicle control effectiveness. This correspondence leads one to believe that the pilot used the

knowledge that the initial portion of the entry is critical and he controls more actively during this segment. The fact that the region around peak g is also a time of high control activity (higher values of ω_c) tends to detract from the generality of this observation.

Retromaneuver

During the retromaneuver, the pilot controls the spacecraft attitude about three axes. Time histories of the attitude error signals (input to the pilot) and the pilot's control signals (output from the pilot), for each of the yaw, roll, and pitch axes, are presented in figure 13. During this

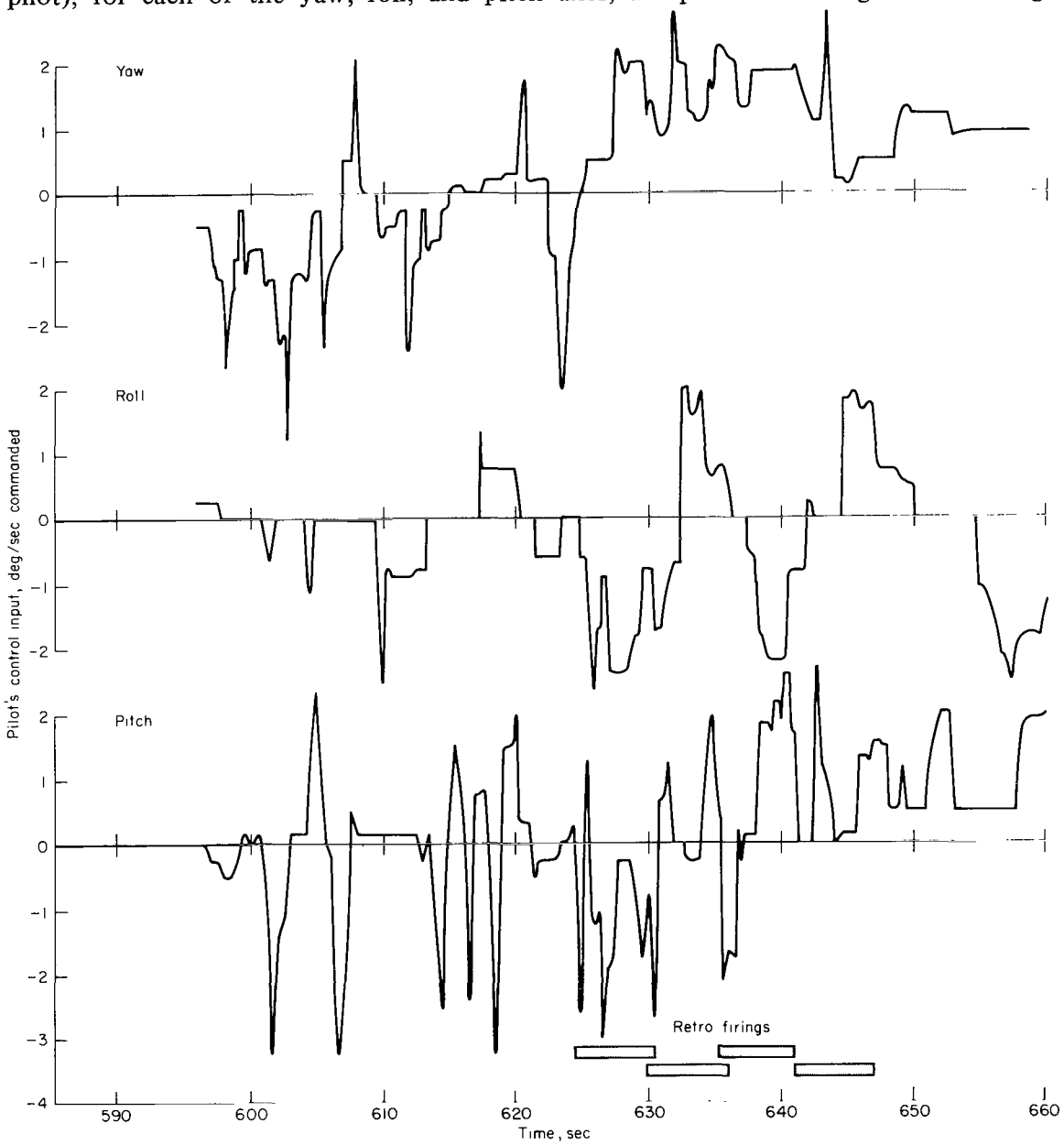

(a) Retromaneuver pilot control signal.

Figure 13.– Time history of data signals during retromaneuver.

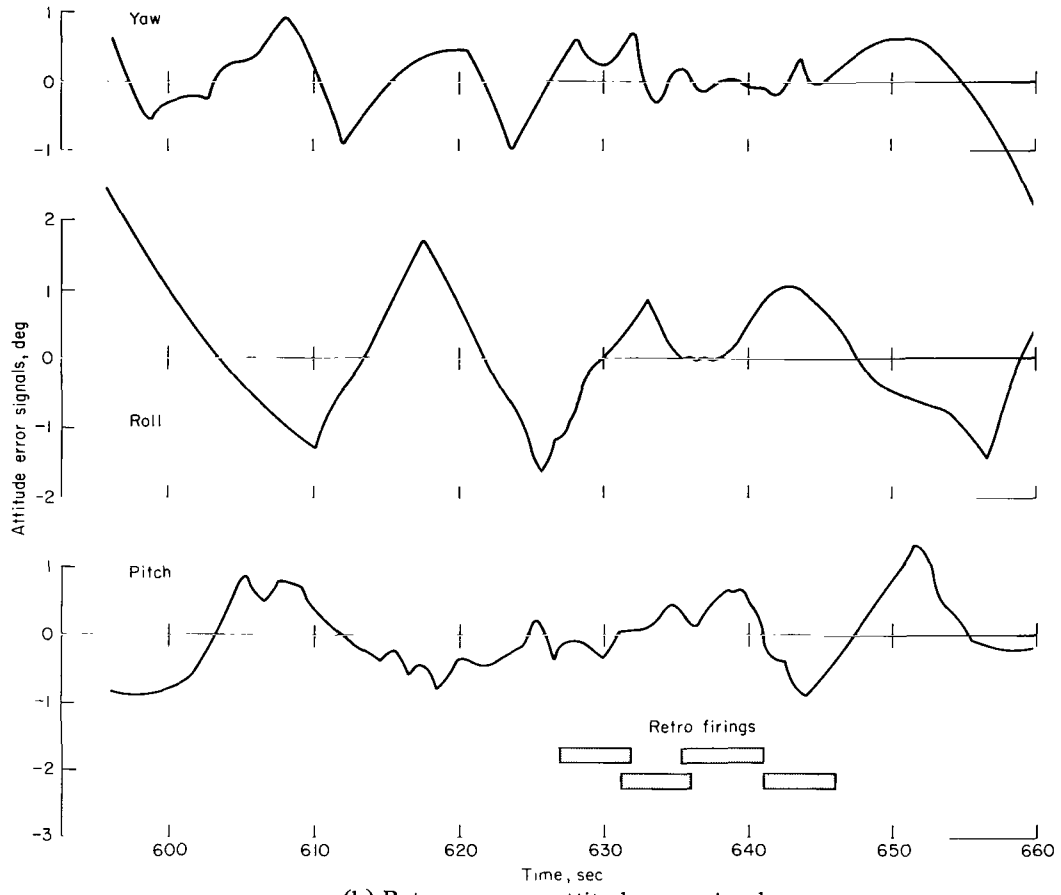

(b) Retromaneuver attitude error signals.

Figure 13.– Concluded.

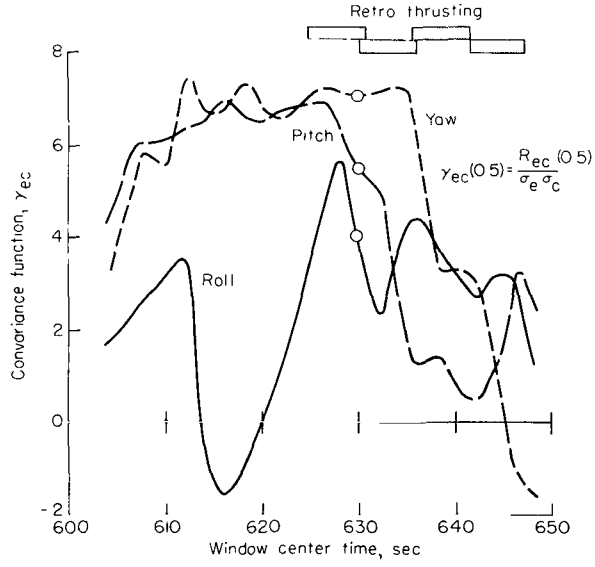

Figure 14.– Variation of the error to control normalized cross-covariance function for each spacecraft axis during the retromaneuver.

maneuver, the spacecraft is being disturbed by the consecutive firing of four retrorockets. The disturbance is predominantly along the X axis of the vehicle with smaller disturbance along the Y and Z axes caused by misalinement of the retrorockets.

Figure 14 shows the time histories of the variation of the normalized cross-covariance functions (error to control) during the retromaneuver. This being a three-axis control maneuver, a separate curve is presented for each axis (pitch, yaw, and roll). Inherent in these computations is the assumption that each of the three axes is controlled independently (in parallel). The sliding window technique was used to compute these values of $\gamma_{ec}(\tau)$ for a window width of 24 sec and a time lag of 0.5 sec.

Consistently high values of $\gamma_{ec}(\tau)$ are apparent for the yaw and pitch axes, while $\gamma_{ec}(\tau)$ for the roll axis varies widely during the maneuver. This may be interpreted to mean that the pilot is conscientiously attempting to keep the yaw and pitch axes under tight control while tolerating large errors in the roll axis. This interpretation is consistent with the appearance of the error time histories presented in figure 13. The error curves show excursions as large as 2° for the roll error but only half that large for the yaw and pitch. It is reasonable to assume that the pilot has assigned different priorities to the yaw, pitch, and roll axes. The criticality of control about the yaw and pitch axes should be apparent in terms of the mission objectives since a large excursion about these axes, during the retrofiring, can result in a miss of the recovery point at splashdown. The control of the roll axis is less critical. The primary purpose of holding inertial roll attitude is to assure that control input about the pitch axis does not couple into the yaw plane and vice versa.

The region about the window center time $t_c = 630$ sec was selected for evaluation and computing the pilot describing functions for each yaw, pitch, and roll axis. This time was chosen because the correlation for each independent axis is high at this time.

The describing function for the yaw axis is evaluated first and presented in figure 15(a) as a frequency response plot. The plot shows the measured describing function for the pilot ($\hat{Y}_p$), the vehicle ($\hat{Y}_c$), and the pilot-vehicle combination ($\widehat{Y_pY_c}$). The orthogonal exponential function method was used to evaluate these describing functions. The estimated transfer function for $\hat{Y}_p$ is essentially a constant gain and a time delay ($\hat{Y}_p = K_p e^{-\tau_p j\omega}$). The transfer function for the effective plant $\hat{Y}_c$ is of the form

$$\hat{Y}_c = K_c e^{-\tau_c j\omega}/j\omega(T_c j\omega + 1)$$

This form of $\hat{Y}_c$ cannot be verified directly from the measured describing function presented in the figure, since the break point ($1/T_c$) of the first order lag is at the high end of the frequency range (above 4 rad/sec). As explained earlier, the low levels of the data signals involved do not permit a valid estimate of the describing functions above 4 rad/sec.

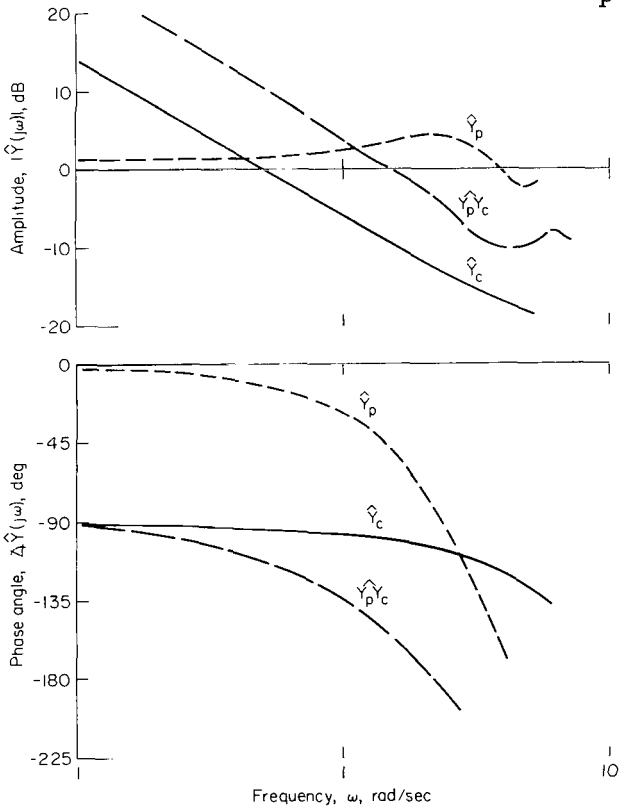

(a) Yaw axis.

Figure 15.– Identification of the describing functions during a segment of the retromaneuver ($t_c = 630$ sec).

As in the example presented for the reentry maneuver, the estimated transfer function for the pilot-vehicle combination can be approximated by the crossover model, $\widehat{Y_pY_c} = \omega_c e^{-\tau_e j\omega}/j\omega$. The crossover frequency ω_c is about 1.2 rad/sec and the effective time delay τ_e is about 0.7 sec for the yaw axis of this retromaneuver. These values of ω_c and τ_e are consistent with the results found in other studies (ref. 17) where the pilot is involved in the complete task of monitoring and controlling about three axes.

The parameter model method was used to estimate the values of gain and time delay in the appropriate expressions for $\hat{Y}_p$, $\hat{Y}_c$, and $\widehat{Y_pY_c}$.

These values are presented in table 1. The coherence measurements corresponding to each of the identifications is also presented in the table for both the parameter model method and a general method. The coherence values from the two identification schemes are in close agreement indicating that the parameters are good linear representations of the processes taken place.

The results from the pitch and roll axis are presented in figures 15(b) and 15(c). For both of these axes the describing function for the pilot-vehicle combination ($\hat{Y}_p\hat{Y}_c$) can be approximated by the crossover model in the frequency region about crossover. The crossover frequency for the pitch and roll axis is about 0.9 and 0.4 rad/sec, respectively, signifying a more sluggish and relaxed control behavior for these two axes than for the yaw axes. An interesting aspect about the control of the pitch axes is that the pilot's gain is higher and he appears to generate lead in the low frequency range. It is not known why the pilot controls in this manner. Control about the roll axis appears to be very relaxed ($\hat{Y}_p\hat{Y}_c$ crossover frequency relatively low). The form of the pilot's transfer function is not well defined from the plot. The pilot's time delay is in excess of 1.2 sec and possibly as high as 1.8 sec, depending on whether an apparent lag term (break point about 1 rad/sec) is assumed for the form of the transfer function. If the form is assumed without the lag ($\hat{Y}_p = K_p e^{-\tau_p j\omega}$), which is the most probable, then the effective time delay would be about 1.8 sec. This large τ_p is again an indication that the pilot allows the error signal to build up substantially before responding.

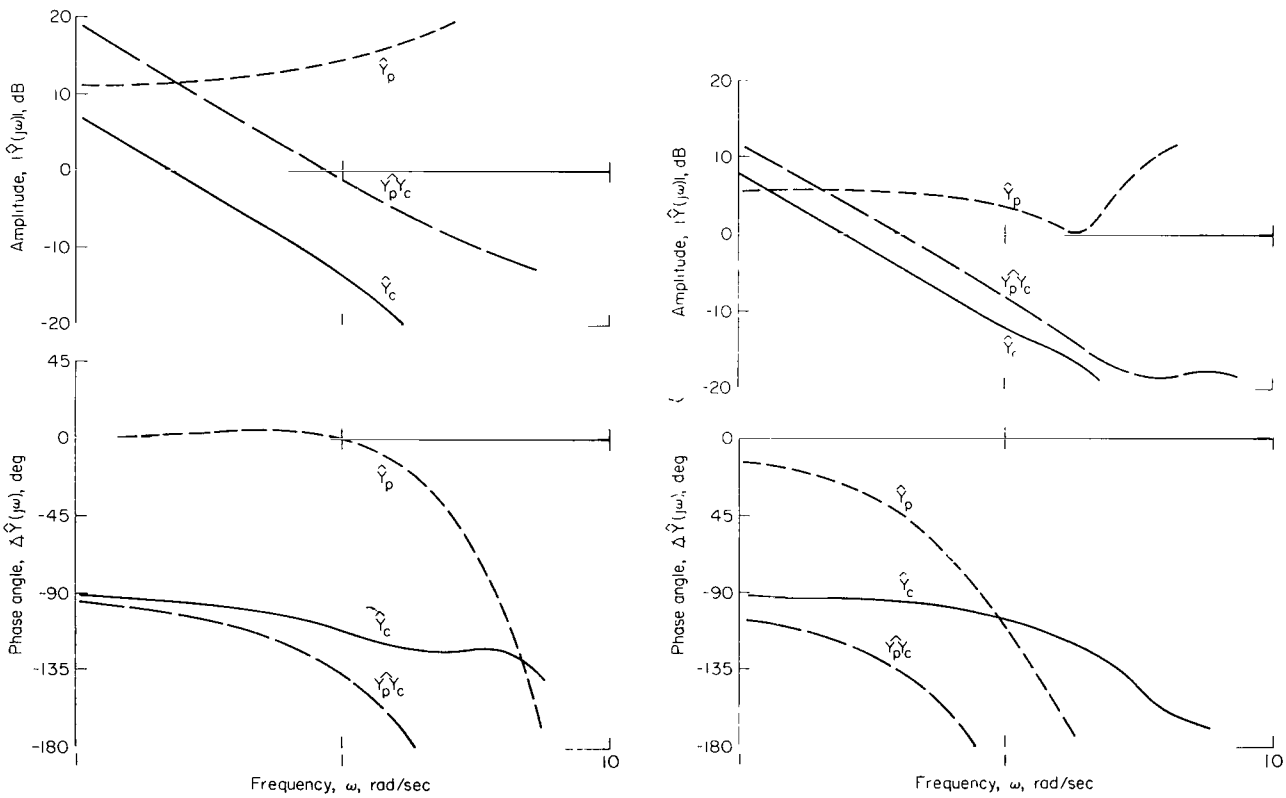

(b) Pitch axis.

(c) Roll axis.

Figure 15.– Concluded.

From a comparison of the $\hat{Y}_p$ for each axis, it is readily apparent that the pilot controls each of the three axes differently. It follows that he has assigned an order of priority to each axis and divided his time and control effort correspondingly. It is suggested that the order of priority is: (1) the yaw axis, (2) the pitch axis, and (3) the roll axis. This sequence of priorities is not fixed for all three axis maneuvers but will be changed to meet the mission objective.

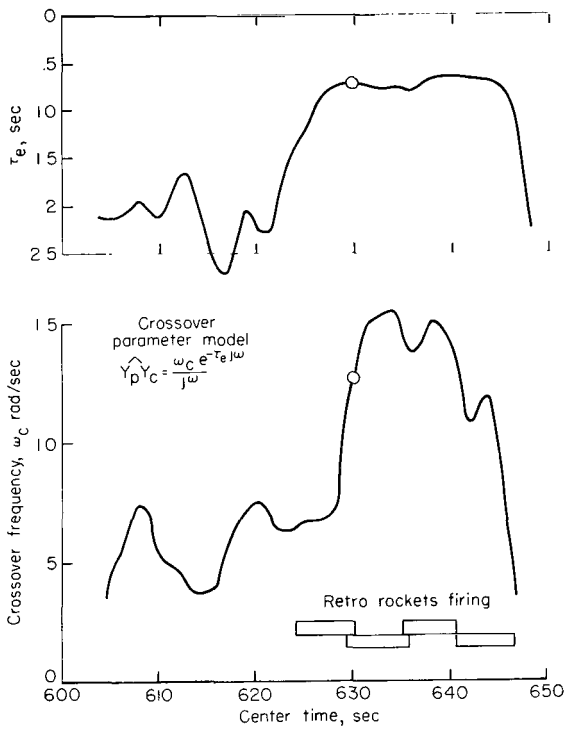

Figure 16.– Variation of the model parameters during the retromaneuver.

It appears from figure 14 that control about the yaw axis contains the best consistent correlation between the pilot's input and output signals. Thus the data for the yaw axis were selected for more extensive analysis to show the pilot's changing control behavior during the retromaneuver. Figure 16 shows time histories of the pilot-vehicle crossover frequency, ω_c, and effective time delay, τ_e, for the period from shortly before the first retrorocket firing until after the last retrorocket firing. The parameter model method was used in conjunction with the "sliding window technique" to obtain these time histories. The parameter model that was used was in the form of the crossover model (eq. (3)). The plots show that prior to the firing of the first retrorocket ω_c is about half a radian per sec and τ_e is nearly 2 sec, indicating that the pilot-vehicle control is sluggish. When the retrorockets begin to fire the control becomes "tight" with ω_c approaching 1.5 rad/sec and τ_e decreasing to 0.5 sec. Toward the end of the maneuver the control once more becomes relaxed at which time ω_c decreases toward zero and τ_e becomes extremely long.

Terminal Phase Initiation Maneuver

The pilot control task during the terminal phase initiation (TPI) maneuver was essentially the same as during the retromaneuver. Specifically, the pilot controls the spacecraft attitude about three axes while the attitude is being disturbed by the firing of the translational thrusters of the spacecraft. Unsymmetrical firing of these thrusters imparts disturbances about the spacecraft axes. The principal difference in the pilot's task between retro and TPI was that the thrust disturbance during the TPI maneuver was an order of magnitude less than during the retromaneuver. It was thought that the difference in thrust magnitude would cause the pilot to modify his control behavior from that demonstrated during the retromaneuver. This proved to be the case.

Time histories of the attitude error signals and the pilot's control output are presented in figure 17. As in the retro case, large excursions of the error signal are present in the roll axis while the pitch and yaw attitude errors are smaller, indicating that the pilot concentrates his effort more on the control of the pitch and yaw axes than on the roll axes.

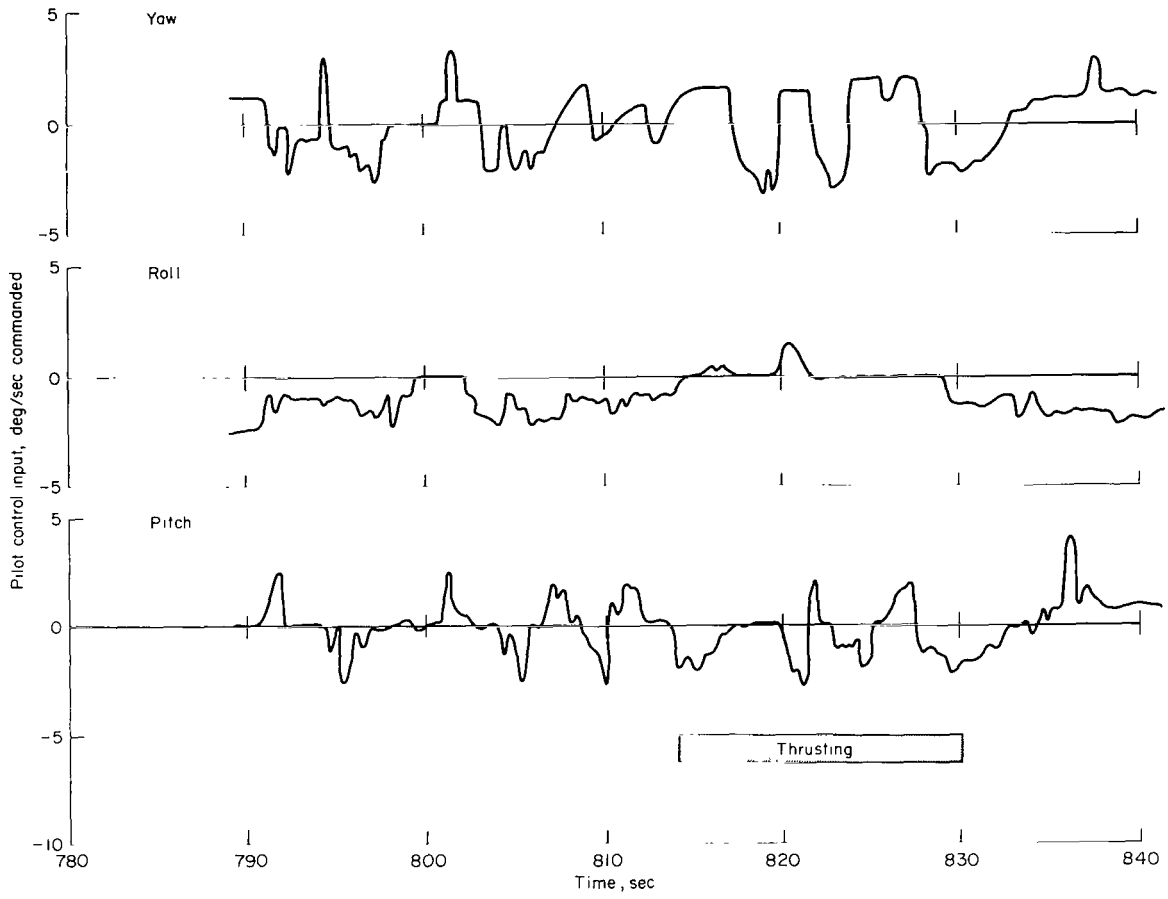

Figure 17.– Time history of terminal phase initiation maneuver.

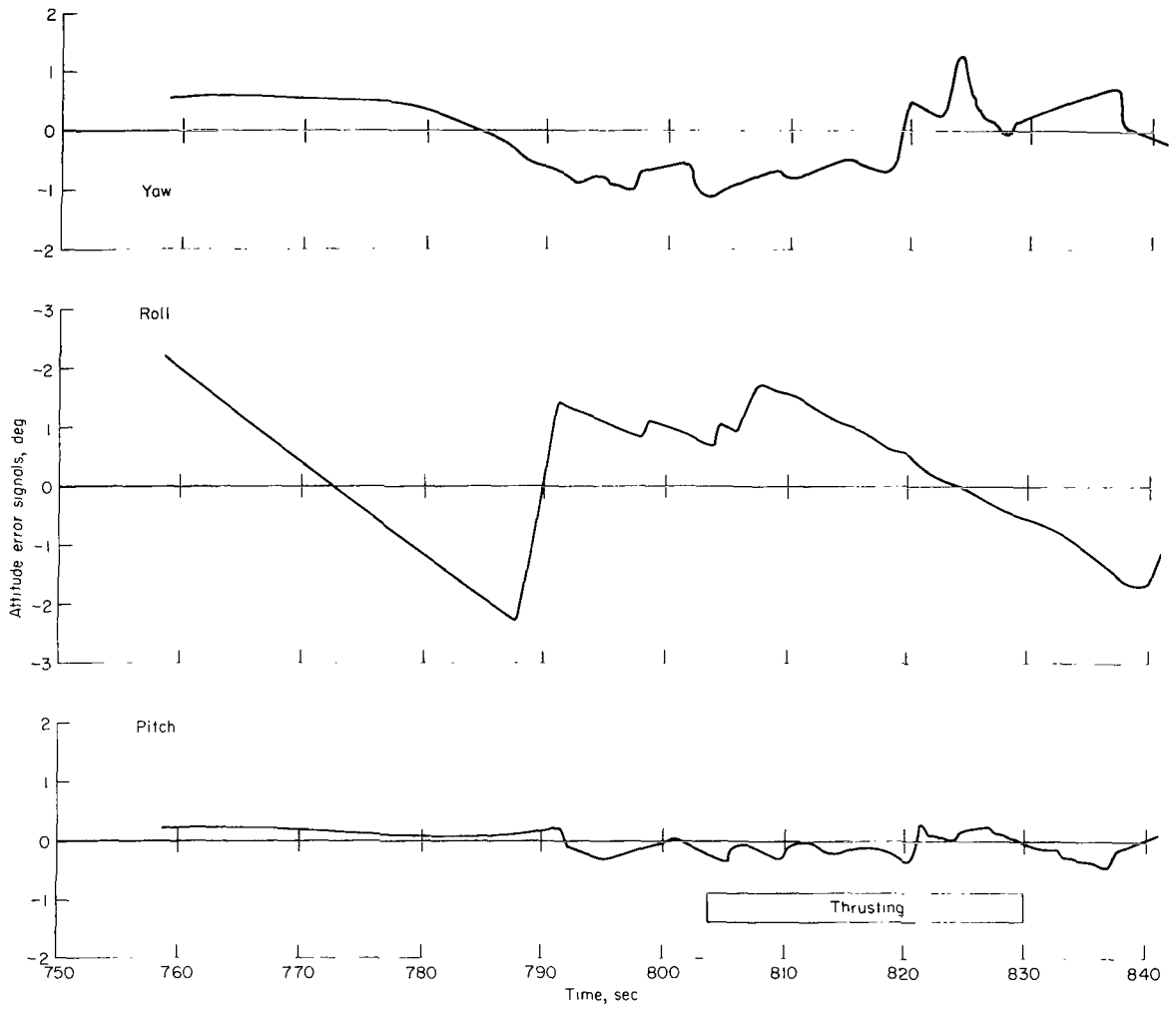

Figure 17.– Concluded.

The time history of the covariance function presented in figure 18 substantiates this appraisal and shows relatively high and consistent values of $\gamma_{ec}(\tau)$ for the pitch and yaw axes and wide variation for the roll axis.

The region about the center time of 797 sec was chosen to evaluate the describing functions for each of the three axes. The describing functions of the pilot, the vehicle, and the pilot-vehicle combination were evaluated by means of the orthogonal exponential function method. The describing functions are presented in figures 19(a), 19(b), and 19(c) for the yaw, pitch, and roll axes, respectively. The parameter model method was used to identify the values for the gain and time delay in the model for the loop components, $\hat{Y}_p$, $\hat{Y}_c$, and $\hat{Y_pY_c}$. The values appear in table 1 for each control axis.

It is immediately evident from table 1 that the pilot's effective time delay is considerably longer for the pitch and yaw axes during this TPI maneuver than during the retro. This is also

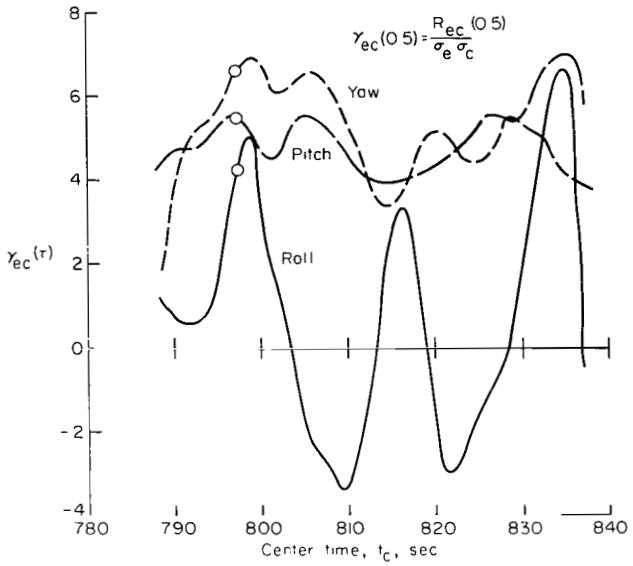

Figure 18.– Variation of the normalized cross-covariance function for each axis during the TPI maneuver.

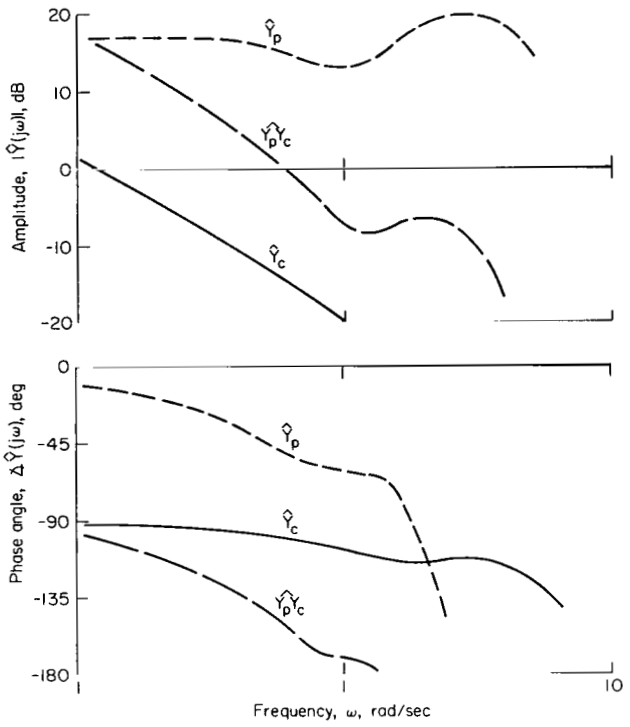

(a) Yaw axis.

Figure 19.

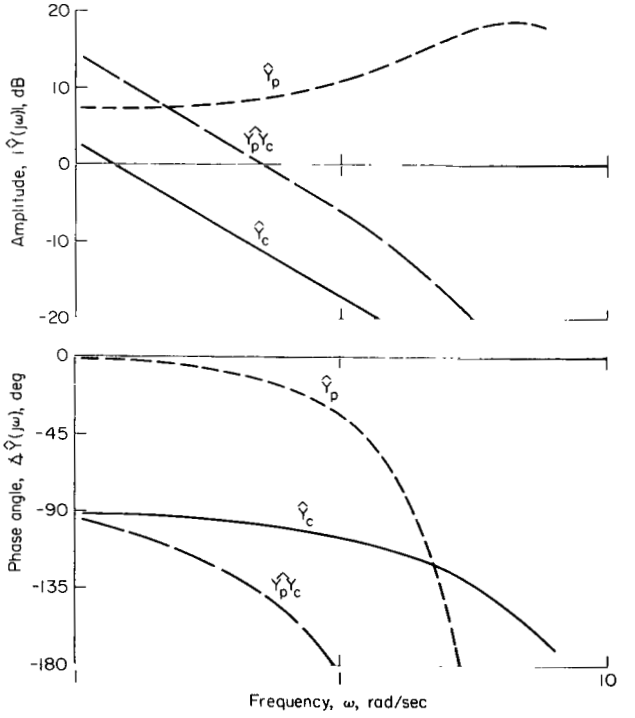

(b) Pitch axis.

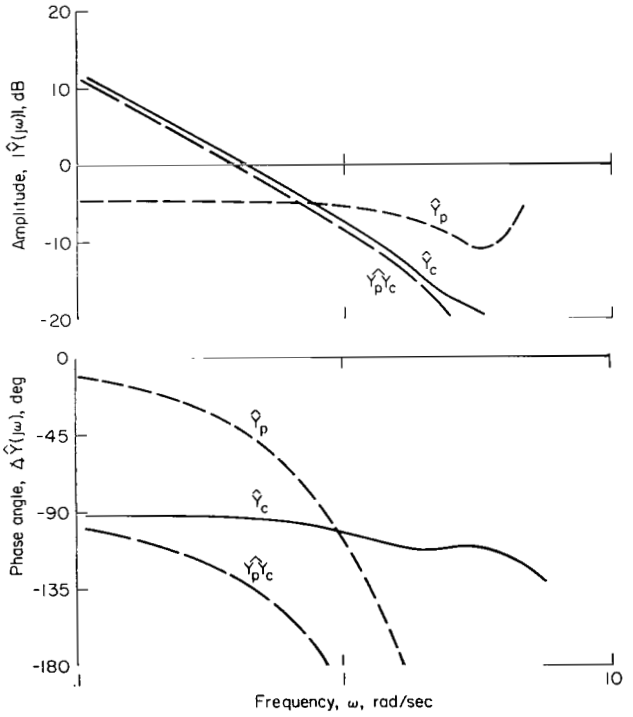

(c) Roll axis.

Figure 19.– Identification of the describing function during a segment of the TPI maneuver (t_c = 797 sec).

evidenced by the larger phase lag present in the describing functions for the pilot (cf. figs. 19 and 15). For each of the axes, the effective time delay was in excess of 1 second. The pilot appears to be in a relaxed mode of operation, probably because of the lower magnitude of the thrust that disturbs the vehicle at a slow rate. The addition of pilot lead in control of the pitch axis is again present for the TPI maneuver as it was for the retromaneuver. The reason for this is not clear.

As a result of the pilot's relaxed mode of operation, the open loop pilot-vehicle crossover frequencies are quite low. For all three axes ω_c is below 0.6 rad/sec and τ_e in excess of 1.0 sec.

It is difficult to establish the order the pilot's control priority for the different axes other than to note that the roll axis is again the least important.

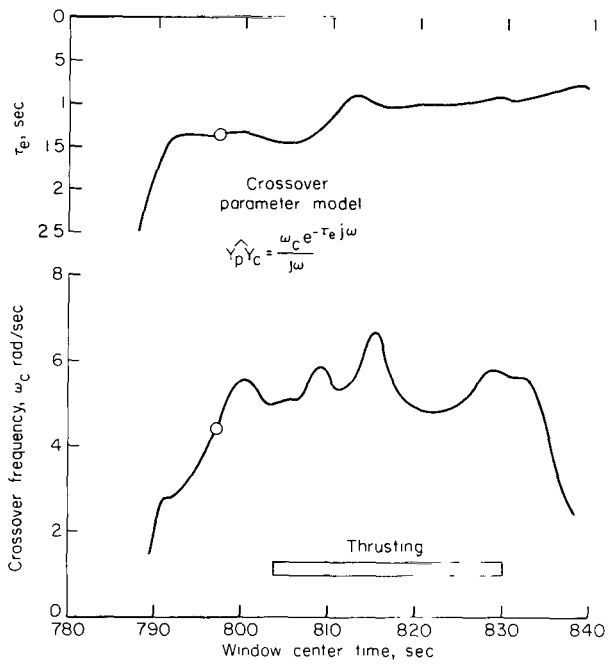

Figure 20.– Variation of the model parameters during the TPI maneuver, yaw axis.

To show that this relaxed mode of control was typical of the pilot's behavior throughout the TPI maneuver, a continuous time history of the pilot-vehicle control behavior was measured for this maneuver. Once again the parameter model method was used to evaluate the crossover frequency and time delay. The crossover model (eq. (3)) represents the process. Time histories of the pilot-vehicle crossover frequency ω_c and effective time delay τ_e were measured for the period from slightly before thrust initiation until after thrust cessation. The results are presented in figure 20. The general trend of the curves is similar to those obtained for the retromaneuver. For instance, during the initial and terminal portions of the maneuver, the crossover frequency is low and the effective time delay is long. This type of operation is to be expected before and after a thrust period for all spacecraft maneuvers. During the period of thrusting the control is relatively more exact with ω_c around 0.6 rad/sec and τ_e about 1.0 sec. In contrast to the results for the retromaneuver (fig. 16) the crossover frequency for the TPI maneuver is consistently less and the effective time delay longer throughout the thrusting period. This difference is an indication of a less demanding task and a more relaxed mode of operation by the pilot.

Comparison of the Three Maneuvers

The estimate of $\hat{Y_p}Y_c(j\omega)$ for the reentry, the retro-, and the TPI maneuvers are compared in figure 21(a). The describing functions are reproduced here from figures 11, 15(a), and 19(a). These selected examples represent the results from three types of maneuvers with two different modes (RRC and RC) of the controlled element. The estimates of $\hat{Y_p}Y_c(j\omega)$ illustrate that during each of the maneuvers the pilot adjusts his dynamics so that in the region of crossover, the pilot-vehicle

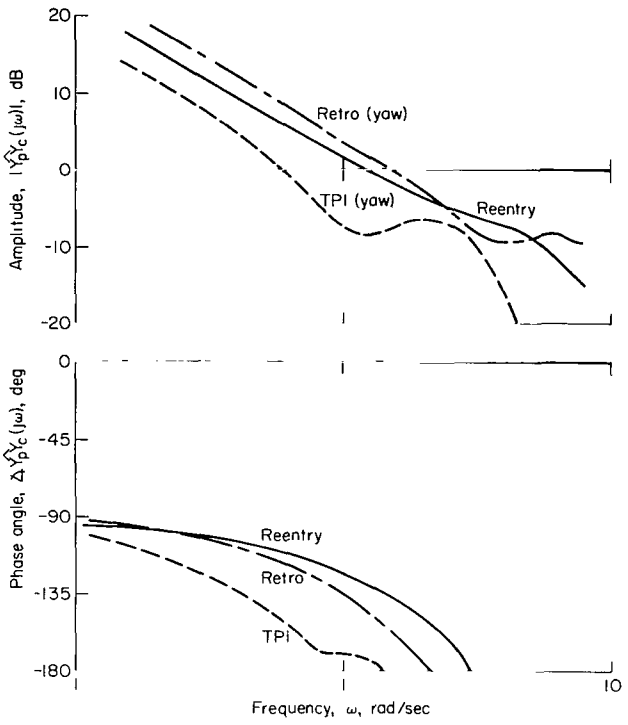

(a) Pilot vehicle, $\widehat{Y_p Y_c}$.

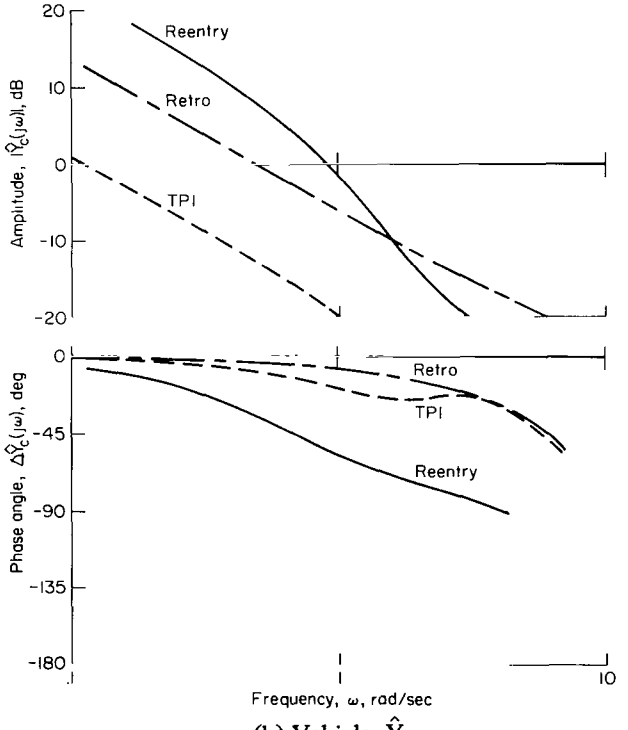

(b) Vehicle, $\hat{Y}_c$.

Figure 21.– Comparison of describing functions for three different space flight maneuvers from Gemini 10.

combination approximates the simple form $\widehat{Y_p Y_c} = \omega_c e^{-\tau e j\omega}/j\omega$. In a variety of previous simulations (refs. 5, 13, and 14) and flight studies (refs. 1 and 2), this simple two parameter crossover model was shown to account for most of the significant pilot-vehicle dynamics in the important crossover frequency region. The nature of the open loop $|Y_p Y_c|_{OL}$ near ω_c determines the dominant closed-loop modes. The system stability is determined by the open-loop gain and phase characteristics near this frequency. For the results presented in figure 21(a) the dynamics are found to have crossover frequencies in the range from 0.6 to 1.5 rad/sec. No doubt these differences in ω_c reflect the difference in the frequency bandwidth of the thrust and aerodynamic disturbances as viewed by the pilot. It was noted in reference 8 that ω_c must exceed the bandwidth of the disturbance for good tracking.

Figure 21(b) shows the estimated describing function of the controlled element (vehicle) for the three maneuvers. Even though these describing functions are linear estimates of an actual nonlinear system they account for up to 76 percent of the power of the control system output signal ($\rho^2 \leqslant 0.76$ for reentry and retro). The apparent differences in the estimate $\hat{Y}_c(j\omega)$ that appear in figure 21(b) are due to two effects. First, the rate feedback gain in the control system increases from the RRC mode during reentry to the RC mode during the retro- and TPI maneuvers. This causes the lag time constant T_c to decrease (break frequency $1/T_c$ increases) and the estimate $\hat{Y}_c(j\omega)$ in the region of crossover goes from approximately an acceleration command system during reentry to approximately a rate command during the retro- and TPI maneuvers.[5]

A second effect is evident when the estimated $\hat{Y}_c(j\omega)$ for the retro- and TPI maneuvers (both are RC mode) are compared. Even though the actual forward gain is the same for the control

[5] For an acceleration command system, $|\hat{Y}_c|$ exhibits a -40 dB/decade slope around ω_c, while for a rate command system $|\hat{Y}_c|$ exhibits a -20 dB/decade slope.

system during the two maneuvers there is an apparent gain change in K_c due to the effect of the nonlinear elements in the systems. This change is a function of the average amplitude of the input signal to the control system. The higher the average amplitude of the input signal, the lower will be the effective gain. The values of control system gain K_c were found to vary from less than 0.1 to as high as 0.7 at different times during the retro- and TPI maneuvers.

CONCLUDING REMARKS

An investigation was made to evaluate and document the pilot and vehicle dynamic response characteristics for three manually controlled maneuvers performed during the Gemini 10 mission. The three maneuvers analyzed were the atmospheric reentry, the retrofire maneuver, and a terminal phase initiation maneuver. The pilot's task was to control the spacecraft attitude manually while being disturbed by either atmospheric or thrust disturbances.

Generally, the flight data records could be characterized as being nonstationary during the total maneuver with short segments of local stationarity. The analysis concentrated on the shorter stationary segments. It was apparent from the records that the pilot could achieve acceptable performance while exhibiting great flexibility in his control behavior. The interaction of the monitoring, control, systems management, and extraneous activities that were part of the pilot's total task would explain the need for this flexibility. Operational manual control systems typically consider these factors in the design and consequently require far less than the operator's limiting control capabilities. This design approach is contrary to that taken in the laboratory (i.e., ref. 15) where the simulated task usually requires the full attention of the pilot. This difference in approach makes the resulting data from flight substantially more difficult to interpret and understand.

In view of the above qualifications, the quantitative values presented in this report should be viewed with some caution. The limited number of runs analyzed and the nonstationary nature of the data caused some reluctance in assigning quantitative values to parameters although in most instances, values were assigned. However, in view of the interest in this area of research and the limited number of results available in the literature from actual space flight missions, it seems appropriate to present these "representative" values which appear in table 1 and in the figures.

In addition, the following general observations are made about the pilot and controlled element behavior:

1. The pilot's response appears to be both nonlinear and time varying in controlling the Gemini spacecraft during actual space flight maneuver. The pilot's response is locally stationary and can be represented in part by a describing function.

2. During the reentry maneuver, the pilot-system crossover frequency appears to be related to the vehicle control effectiveness (capability to change the flight path) and uncorrelated with the magnitude of the reentry acceleration.

3. During control of the three-axis maneuvers (retro- and TPI) the pilot appears to assign priorities to each of the axes and to divide his time and control effort correspondingly. The

indication is that he attaches less importance to the control of the roll axis and at times drops all attention to this particular axis while directing his attention to control of the pitch and yaw axes.

4. The Gemini manual control system in either the reentry rate command mode or the rate command mode is highly damped and easily controlled. Adequate control of the system does not require the full attention of the pilot to achieve the level of performance required for mission success.

Ames Research Center
National Aeronautics and Space Administration
Moffett Field, Calif., 94035, December 21, 1971

APPENDIX A

NORMALIZED CROSS–COVARIANCE FUNCTION

As used in this study, the covariance function gives a preliminary estimate of the linear correlation between the input and output records of the system to be identified (pilot or vehicle). A high value of linear correlation would indicate a segment of the data record that would be amenable to further analysis. A low or negative value of $\gamma(\tau)$ indicates the record segment would yield poor results were an attempt made to identify the system relating the two signals. These points will be discussed in more detail in this appendix.

The basic definition of the normalized cross-covariance function as given in reference 14 is

$$\gamma_{xy}(\tau) = \frac{C_{xy}(\tau)}{\sqrt{C_x(0)C_y(0)}} \tag{A1}$$

where $C_{xy}(\tau)$ is the cross-covariance function between two signals X(t) and Y(t); and $C_x(0)$ and $C_y(0)$ are the autocovariance function at zero time displacement. These three functions are defined by the following expressions which also show their relationship to the more familiar correlation coefficients

$$C_{xy}(\tau) = \lim_{W\to\infty} \frac{1}{W}\int_0^W [X(t) - \mu_x][Y(t+\tau) - \mu_y]\,dt$$

$$= R_{xy}(\tau) - \mu_x\mu_y$$

$$C_x(\tau) = \lim_{W\to\infty} \frac{1}{W}\int_0^W [X(t) - \mu_x][X(t+\tau) - \mu_x]\,dt$$

$$= R_x(\tau) - \mu_x^2$$

$$C_y(\tau) = \lim_{W\to\infty} \frac{1}{W}\int_0^W [Y(t) - \mu_y][Y(t+\tau) - \mu_y]\,dt$$

$$= R_y(\tau) - \mu_y^2$$

where W is the length of the data sample, μ_x and μ_y are the mean values of the two signals X(t) and Y(t); $R_x(\tau)$ and $R_y(\tau)$ are autocorrelation functions and $R_{xy}(\tau)$ is the cross-correlation function. It is always possible to evaluate and extract the mean values from the signals X(t) and Y(t) to obtain the zero mean valued signals x(t) and y(t). The covariance and correlation functions of the new signals are then equivalent (i.e., $C_{xy}(\tau) = R_{xy}(\tau)$, $C_x(\tau) = R_x(\tau)$ and $C_y(\tau) = R_y(\tau)$. The normalized cross-covariance function can then be written as

$$\gamma_{xy}(\tau) = \frac{R_{xy}(\tau)}{\sqrt{R_x(0)R_y(0)}} \tag{A2}$$

The autocorrelation function at zero time displacement R(0) is identically equal to the variance (σ^2) of the signal. Thus it follows the $\gamma_{xy}(\tau)$ is simply

$$\gamma_{xy}(\tau) = \frac{R_{xy}(\tau)}{\sigma_x \sigma_y} \tag{A3}$$

Thus, the normalized cross-covariance function is directly related to the cross-correlation function. The cross-correlation function for two sets of random data (i.e., x(t) and y(t)) describes the general dependence of the values of one set of data on the other (see ref. 14). Thus the function $\gamma_{xy}(\tau)$ gives a measure of the degree of linear dependence between x(t) and y(t) for a displacement of τ in y(t) relative to x(t). This function $\gamma_{xy}(\tau)$ is also known as the correlation coefficient. The values of $\gamma_{xy}(\tau)$ lie between -1 and +1. Random variables x(t) and y(t), whose correlation coefficient is zero, are said to be uncorrelated. The value $\gamma_{xy}(\tau) = +1$ indicates that the two data records are perfectly correlated. If $\gamma_{xy}(\tau)$ should be -1.0, this would indicate that the output signal was perfectly correlated with the input signal but of opposite sign. In the case of human pilot's input-output relationship, a negative value of $\gamma_{xy}(\tau)$ indicates that the pilot's control stick outputs are backward (control reversal). Normally $\gamma_{xy}(\tau)$ for human pilot input output relationship fall in the range from zero to +1.0.

In this study the principal motivation for the use of the covariance function was to provide a "quick look" capability for evaluating long data records. In order for a parameter to be used effectively for this purpose, it should meet the following criteria.

(1) The parameter should provide a quantitative measure of the relative quality of different segments of the data record. (The magnitude of the parameter $\gamma_{xy}(\tau)$ will influence our decision on whether to proceed with a thorough analysis.)

(2) In addition, the use of the parameter should be easy to understand and require a minimum of computation.

The brief discussion presented above and a more extensive proof presented in reference 14 indicates that $\gamma_{xy}(\tau)$ meets the first of these criteria. An example computation will show that the second criterion can be met as well.

We will next present and discuss the results of example computations of the cross-covariance function $C_{xy}(\tau)$. We will first indicate an efficient manner of computing this parameter and then show its relationship to the linear coherence function, ρ^2, which is a measure of the linearly correlated portion of the output.

The examples presented are from a segment of the data record of the retrofire of the Gemini 10 mission. For a 24-sec segment of the data the normalized cross-covariance function equation (A3) is computed to evaluate the linear dependence between the pilot's input and output signals (error to control), the vehicle input and output signals (control to rate), and the combination pilot-vehicle input to output signals (error to rate). Values are computed for distinct time lags for the range of τ from -1.5 to +1.5 sec. The faired results for the three variations are presented in sketch (a). The significant features of these plots are that they are continuous functions of the time lag τ, and they reach a maximum in the positive time domain ($+\tau$). The characteristics of these curves enable us to reduce the number of computations required to obtain an estimate of the peak value of $\gamma_{xy}(\tau)$. The peak value is of primary interest, for it indicates the τ for which maximum correlation exists. It is immediately apparent that no computations are required for the negative time domain ($-\tau$). Since we are always concerned with physically realizable systems, the peak value of $\gamma_{xy}(\tau)$ will always appear in the positive time domain. Because of the smoothly varying nature of this parameter it appears probable that an evaluation over a wide lag time range may not be necessary either. If a good estimate of the peak value of $\gamma_{xy}(\tau)$ could be determined from a single computation for each time segment of the data record, the total number of computations would be reduced dramatically and the usefulness of the parameter enhanced. This process proved quite practical. For example, in sketch (a) note that any value of τ between 0.14 and 0.81 sec gives an estimate of $\gamma_{ec}(\tau)$ within 10 percent of the peak value. Also for the curve of $\gamma_{er}(\tau)$, values for τ from 0.47 to 1.14 sec result in an estimate of the peak value of $\gamma_{er}(\tau)$ within 10 percent. Furthermore, for the control to rate signals, $0.0 < \tau < 0.3$ results in an estimate of $\gamma_{cr}(\tau)$ within 10 percent of the peak value. Thus it appears that certain representative values of τ can be selected and a good estimate of the peak values of $\gamma_{xy}(\tau)$ can be obtained from a single computation. For the example presented in the text of this report the following representative values of lag time τ were chosen for calculating the covariance functions.

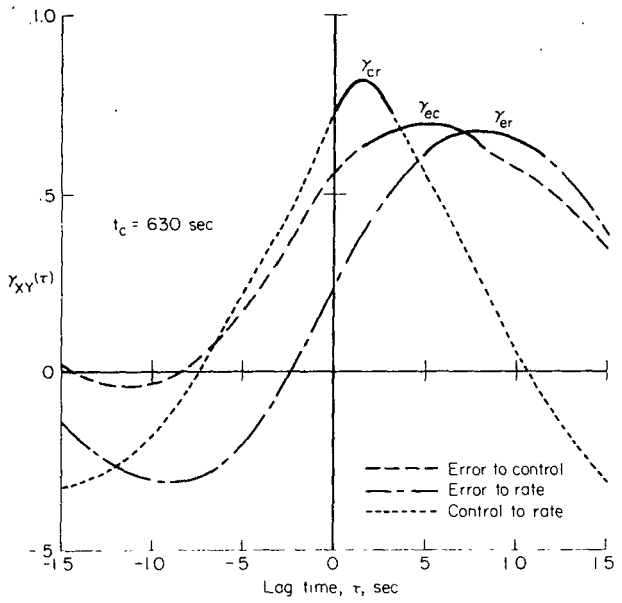

Sketch (a)

$\tau = 0.5$ input-output signals of the pilot (error to control)

$\tau = 0.2$ input-output signals of the vehicle (control to rate)

$\tau = 0.7$ input-output signals of the pilot-vehicle combination (error to rate)

For time segments where the values of τ given above are not truly representative of the actual time lags of the systems, a measure of the parameter $\gamma_{xy}(\tau)$ will still provide a relative evaluation of adjacent time segments. The computed values of $\gamma_{xy}(\tau)$ may be less than the peak values but will still be useful in locating "good tracking" segments. To clarify this point, an example computation

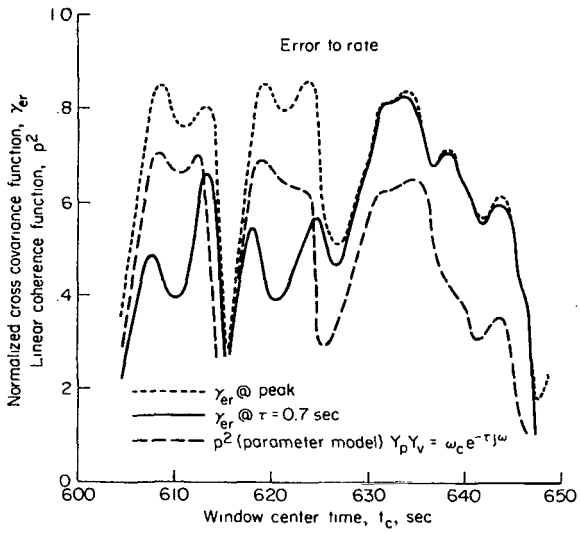

Sketch (b)

is presented in sketch (b). Again the data from the retromaneuver are used. The sliding window technique described in appendix B is used to select the segments of the data records. Three time histories are presented in sketch (b). Two curves show the variations of the normalized cross covariance function for the vehicle attitude error to rate signals. One curve is for $\gamma_{er}(\tau)$ at $\tau = 0.7$ sec (the representative value) and the other curve for the peak value of $\gamma_{er}(\tau)$ (τ selected at each data segment to give maximum $\gamma_{er}(\tau)$. The time histories of the two covariance functions show that during the initial part of the maneuver there is a wide discrepancy between $\gamma_{er}(0.7)$ and $\gamma_{er}(\tau)$ at the peak. Nevertheless there is still a positive indication from the time history of $\gamma_{er}(0.7)$ of the location of the good tracking segments. During the latter part of the maneuver (beyond $t_c = 630$ sec) the two curves nearly coincide. The coincidence occurs when the actual lag of the system move nearly agrees with $\tau = 0.7$ sec. Thus for "quick look" purposes, $\gamma_{xy}(\tau)$ computed at a representative value of τ is adequate for evaluating the tracking records.

The third curve on the plot shows the variation of the linear coherence function ρ^2 resulting from an identification of the system which relates the two signals. The parameter model $\hat{Y}_pY_v = \omega_c e^{-\tau e j\omega}$ is used in the identification computation. The curve of ρ^2 parallels that for the peak value of $\gamma_{er}(\tau)$ throughout the maneuver and shows a relationship to the curve of $\gamma_{er}(0.7)$ which is similar to that explained above for $\gamma_{er}(\tau)$ at the peak; that is, for periods when ρ^2 is high, $\gamma_{er}(0.7)$ is also high. This point is significant when we consider the computational process involved in obtaining values of γ_{er} and ρ^2. The process of obtaining $\gamma_{er}(0.7)$ requires far fewer mathematical computations than is required to compute values of ρ^2.

APPENDIX B

SLIDING WINDOW TECHNIQUE

In this appendix we will outline a computational technique for evaluating continuous short time averages. This is referred to as the sliding window technique. An example computation using this method is given and discussed. The application of the technique for evaluating stationarity of the data, determining time histories of the covariance function, and for identifying describing functions is indicated.

The sliding window technique is simply a process for selecting short segments of a long data record for analysis purposes. This is accomplished by subdividing the record of data into a number of shorter, overlapping segments. For each time segment a short time average computation is made. As an example, consider two sample records such as shown in sketch (c). These can be any time histories of the input and output of a physical system (i.e., pilot, vehicle) during the period from time = T_1 until time = T_2.[1] A segment of each record is viewed through a "window" of width W, which is less than the total record length. For the position of the window a short time average computation is made. This computation could include the mean and mean square values of each signal, the covariance function between the signals or the describing function of the system that relates the two signals. The window is then moved to a new position where the computation is again made. This process is continued until the entire record has been scanned. Adjacent window position may overlap. The results are plotted versus the center time of the window (t_c). In this manner we generate a continuous short time average of the computed parameters.

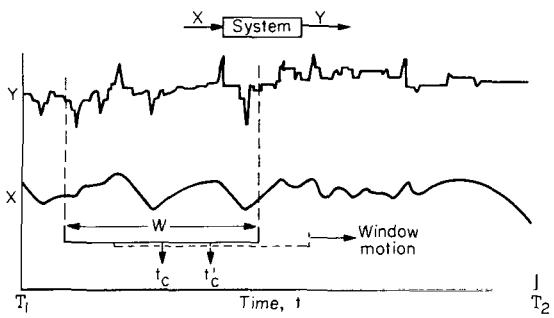

Sketch (c)

As an example, assume that we would like to evaluate the sample mean squared value of the two signals that appear in sketch (c). The computations are to use the discrete form of the equation for evaluating the mean squared value,

$$\Psi^2(t_c) = \frac{1}{N}\sum_{n=1}^{N}(\lambda_n)^2 \qquad T_1 + \frac{W}{2} \leqslant t_c \leqslant T_2 - \frac{W}{2} \tag{B1}$$

[1] The example records shown in sketch (c) are actually the input and output records of the pilot during the retrofire maneuver (yaw axis). The records are typical of those analyzed in this study.

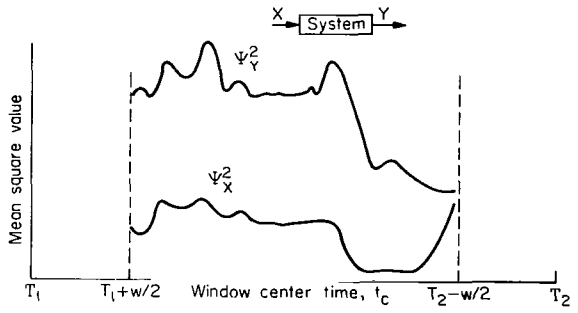

Sketch (d)

where N is the number of data samples included in the window ($N = W/\Delta t$); λ_n are the data values (X_n, Y_n); and t_c is the center time of the window. The results would appear as shown in sketch (d). For the computations presented in sketch (d) and most of the computations presented in this study a data window of 24 sec was selected. The data window was translated in time at increments of 1.0 sec. The resulting data have been faired.

Stationarity of the data– The plots that appear in sketch (d) allow insight into the quality of the data which is not available if a single average were computed for the total record length. Specifically, the process provides a useful test for data stationarity. A simple and commonly used test is that of simple visual observation of the mean or mean squared value over a period of time. Stationarity requires that the mean and mean squared values be invariant with translation in time. The theoretical ideas and processing techniques used in this study do not apply when the data are nonstationary (i.e., statistical properties change with time). The difficulty with this test for stationarity described above is that there are no quantitative parameters in the test on which a decision is based. Acceptance or rejection is purely qualitative. Nevertheless, this procedure is probably one of the most effective in performing a preliminary analysis of a record that probably is not strictly stationary. If it can be shown that the average mean square value of the signal is varying "slowly," the physical process may be assumed to be locally stationary. The statistical processing techniques of this study could then be used. The best that may be obtained is the establishment of a reasonably stable level of stationarity for a period of time. In this study the sliding window technique was used to select and analyze certain 24 sec segments for which the data were observed to be locally stationary.

REFERENCES

1. Newell, F. D.: Human Transfer Characteristics in Flight and Ground Simulation for the Roll Tracking Task. Tech Rep. AFFDL–TR–67–30, USAF, April 1968.

2. Kuehnel, Helmut A.: Human Pilot's Dynamic Response Characteristics Measured in Flight and On a Nonmoving Simulator. NASA TN D–1229, 1962.

3. Seckel, E.; Hall, I. A. M.; McRuer, D. T.; and Weir, D. H.: Human Pilot Dynamics Response in Flight and Simulator. WADC–TR–57–520, Aug. 1958.

4. Isakov, P. I.; Popov, V. A.; and Khachatur'yants, L. S.: Problem of Evaluating Physical Fitness of Cosmonauts. NASA TTF–9593, 1965.

5. Wingrove, R. C.; and Edwards, F. G.: A Technique for Identifying Pilot Describing Functions From Routine Flight-Test Records. NASA TN D–5127, 1969.

6. Wingrove, R. C.; Edwards, F. G.; and Lopez, A. E.: Some Examples of Pilot/Vechicle Dynamics Identified From Flight Test Records. IEEE Trans. on Man-Machine Systems, MMS–10, no. 4, Dec. 1969.

7. Wingrove, R. C.; and Edwards, F. G.: Measurement of Pilot Describing Functions From Flight Test Data With an Example From Gemini X. IEEE Trans. on Man–Machine Systems, MMS–9, pp. 49–55, Sept. 1968.

8. McRuer, Duane; and Jex, Henry: A Review of Quasi-Linear Pilot Models. IEEE Trans. on Human Factors in Electronics, HFE–8(3), 1967.

9. Elkind, Jerome I.: Further Studies of Multiple Regression Analysis of Human Pilot Dynamic Responses. A Comparison of Analysis Techniques and Evaluation of Time Varying Measurements. ASD–TDR–63–618, March 1964.

10. Goodman, T. P.; and Reswick, J. B.: Determination of System Characteristics From Normal Operating Records. Transactions of the ASME, vol. 78, Feb. 1956, pp. 259–268.

11. Wierwille, Walter W.; and Gagne, Gilbert A.: A Theory for the Optimal Deterministic Characterization of the Time Varying Dynamics of the Human Operator. NASA CR–170, 1965.

12. Adams, James J.; Bergeron, Hugh P.; and Hurt, George J., Jr.: Human Transfer Functions in Multi-Axis and Multi-Loop Control Systems. NASA TN D–3305, 1966.

13. Wingrove, R. C.: Comparison of Methods for Identifying Pilot Describing Function From Closed-Loop Operating Records. NASA TN D–6235, Sept. 1970.

14. Bendat, J. S.; and Piersol, A. G.: Measurement and Analysis of Random Data. John Wiley and Sons, Inc., 1966.

15. McRuer, Duane; and Graham, Dunstan: Human Pilot Dynamics in Compensatory Systems. Tech. Rep. AFFDL–TR–65–15, USAF, July 1965.

16. Sadoff, Melvin: Effects of High Sustained Acceleration on Pilot's Performance and Dynamic Response. NASA TN D–2067, 1964.

17. Clement, W. F.; Jex, H. R.; and Graham, D.: Application of a System Analysis Theory for Manual Control Displays to Aircraft Instrument Landing. Paper presented at 4th Annual NASA–University Conference on Manual Control, Univ. Michigan, March 1968.

NASA-Langley, 1972 —— 5 A–3877

"The aeronautical and space activities of the United States shall be conducted so as to contribute . . . to the expansion of human knowledge of phenomena in the atmosphere and space. The Administration shall provide for the widest practicable and appropriate dissemination of information concerning its activities and the results thereof."

—NATIONAL AERONAUTICS AND SPACE ACT OF 1958

NASA SCIENTIFIC AND TECHNICAL PUBLICATIONS

TECHNICAL REPORTS: Scientific and technical information considered important, complete, and a lasting contribution to existing knowledge.

TECHNICAL NOTES: Information less broad in scope but nevertheless of importance as a contribution to existing knowledge.

TECHNICAL MEMORANDUMS: Information receiving limited distribution because of preliminary data, security classification, or other reasons.

CONTRACTOR REPORTS: Scientific and technical information generated under a NASA contract or grant and considered an important contribution to existing knowledge.

TECHNICAL TRANSLATIONS: Information published in a foreign language considered to merit NASA distribution in English.

SPECIAL PUBLICATIONS: Information derived from or of value to NASA activities. Publications include conference proceedings, monographs, data compilations, handbooks, sourcebooks, and special bibliographies.

TECHNOLOGY UTILIZATION PUBLICATIONS: Information on technology used by NASA that may be of particular interest in commercial and other non-aerospace applications. Publications include Tech Briefs, Technology Utilization Reports and Technology Surveys.

Details on the availability of these publications may be obtained from:

SCIENTIFIC AND TECHNICAL INFORMATION OFFICE

NATIONAL AERONAUTICS AND SPACE ADMINISTRATION

Washington, D.C. 20546